



Topographic expressions of mantle dynamics in the Mediterranean

Claudio Faccenna^{a,b,c,*}, Thorsten W. Becker^{b,c}

^a Lab. Experimental Tectonics, Department of Science, Univ. Roma TRE, Italy

^b Department of Geological Sciences, Jackson School of Geosciences, The University of Texas at Austin, USA

^c Institute for Geophysics, Jackson School of Geosciences, The University of Texas at Austin, USA



ABSTRACT

The surface of the Earth is the ever-changing expression of the dynamic processes occurring at depth and at or above its surface. However, our ability to “read” landscapes in terms of their underlying tectonic or climatic forcing remains rudimentary. During the last decade, particular attention has been drawn to the deep dynamic contributions to topography, related to the stresses that are produced at the base of the lithosphere by mantle convection, and their relevance compared to the (iso)static component of topography. Here, we use examples from the Mediterranean and estimate residual and dynamic topography. We then compare those with surface uplift from geology for specific regions to disentangle the dynamic from the static components. Considering the different topographic signatures of tectonic processes (e.g. actual, residual, and dynamic topography as well as uplift rates) jointly provides a powerful way to distinguish between the contributions of mantle, crustal, and surface processes. Such an approach might bring us closer to reading topographic expressions in terms of their geological cause.

1. Introduction

The surface of the Earth is the ever-changing expression of the dynamic processes at depth or at and above its surface, but our ability to “read” landscapes in terms of their underlying tectonic or climatic forcing is limited. There are three main processes contributing to Earth's topography: mantle convection, crustal and lithosphere deformation, including volcanism and magmatic underplating, and surface mass transfer due to erosion/sedimentation, or water and ice (un)loading changes related to natural or anthropogenic sources (Fig. 1).

Geodynamic processes such as mantle convection produce horizontal motions of the Earth's surface, but also drive plate tectonics and crustal deformation at plate boundaries which manifests itself as vertical motion through the resulting isostatic equilibrium of thickened or thinned crust. Tectonically uplifted rock is sculpted and eroded by geomorphic processes such as winds, rivers, hillslope and glacial transport, which are themselves are modulated by climate (e.g., Whipple, 2009). Topography is the product of the interaction and feedback between those processes occurring over diverse time and spatial scales (e.g., Forte, 2000; Braun, 2010; Flament et al., 2013).

In general, topography can be described as the sum of an isostatic and a dynamic component. The isostatic elevation depends only on the buoyancy of the lithosphere (e.g., Holmes, 1944). The dynamic topography, i.e. the non-isostatic component, is generated by stress at the base of the lithosphere (e.g., Le Stunff and Ricard, 1995; Hager et al., 1985; Hager and Richards, 1989; Mitrovica et al., 1989a, Mitrovica et al., 1989b; Gurnis, 1990; Le Stunff and Ricard, 1995; Panasyuk and

Hager, 2000; Forte, 2000; Braun, 2010; Flament et al., 2013; Rowley et al., 2013a, Rowley et al., 2013b; Winterbourne et al., 2014; Arnould et al., 2018. Surface uplift rate, defined as the time derivative of the elevation of the Earth's surface, similarly, has sources from the deep mantle, lithosphere, and crust (Fig. 1a).

Joint observations of topography, surface and rock uplift rate could help to differentiate between the processes. Rock uplift is different from surface uplift as the former refers to the movement of a rock toward the surface, whereas the latter refers to variation of surface elevation, in other words surface uplift is equal to rock uplift minus erosion. Climatic variability in the system affects surface erosion and then contributes to tectonic erosion and rock uplift (e.g., Wager, 1933; Holmes, 1944; England and Molnar, 1990; Willett, 1999; Beaumont et al., 2000; Willett et al., 2001; Bonnet and Crave, 2003; Whipple and Meade, 2006, Bishop, 2007).

To distinguish between the isostatic and dynamic components, it is necessary to estimate the density structure of the lithosphere and the motion of the mantle. To resolve the factors contributing to uplift rate, it is necessary to estimate erosion and sedimentation rates, crustal thickening or thinning rates and transient components of dynamic topography, including the isostatic adjustment from ice sheet melting and water loading (e.g., England and Molnar, 1990). Those process may have different amplitudes and rates, and their superimposition may complicate interpretations (Fig. 1b).

In this paper, we discuss topographic signals as the result of the contributions of mantle, crustal, and surface processes. We suggest that the different kinds of topography signals may be used to distinguish the

* Corresponding author at: Department of Geological Sciences, Jackson School of Geosciences, The University of Texas at Austin, USA
E-mail address: faccenna@uniroma3.it (C. Faccenna).

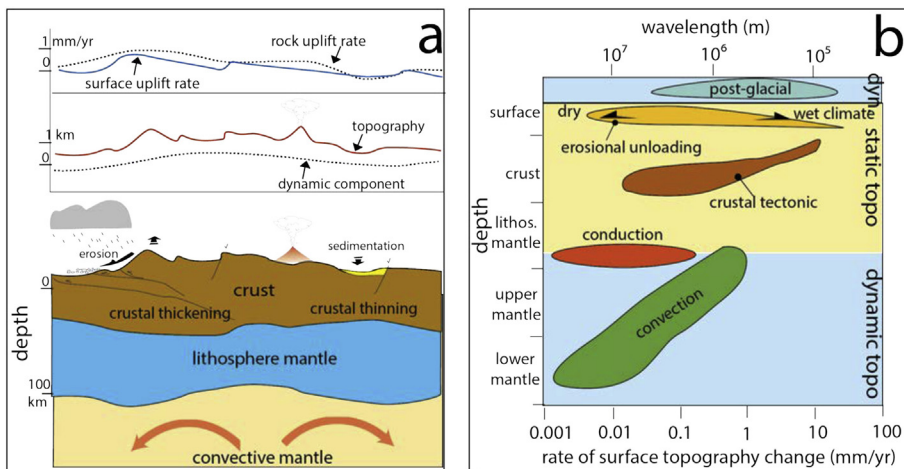


Fig. 1. a) Cartoon (not to scale) showing the contribution of different dynamic (blue) and isostatic (yellow) processes operating to shape the topography; b) Synopsis showing the approximate rate and wavelength of topography variation for processes operating at different depth. (For interpretation of the references to colour in this figure legend, the reader is referred to the web version of this article.)

tectonic processes that are active in the region. To illustrate this approach, we use as an example the Mediterranean region, which has been the subject of numerous studies to investigate mantle structure as well as the tectonic and geomorphic evolution.

2. Topography, residual topography, and dynamic modeling

Understanding the origin of topography requires the following constraints:

- Topography and its variation over time (i.e. uplift);
- Residual topography (i.e. non-isostatic topography from a lithospheric correction);
- Dynamic topography (due to active mantle flow).

In the following we illustrate these constraints for the Mediterranean.

2.1. Topography and its variation over time

While actual, present-day surface topography is ever more readily available with increasing resolution, the rate of topography change is still poorly constrained. The longevity of GPS observational networks and advances in InSAR and other methods of satellite geodesy now provide a robust estimate of the short-term variation of the surface elevation over specific areas. The western – central European Mediterranean in particular is fairly well covered by permanent GPS stations (Fig. 2).

Some of the geodetic uplift features seen in Fig. 2a have been discussed previously (Serpelloni et al., 2013), including a positive signal over the Alps (cf. Sternai et al., 2019, for a review), the Southern Apennines and Sicily (cf. Faccenna et al., 2014a; Faccenna et al., 2014b), NW Iberia, the Valencia Trough, and the Iberian chain on the Iberian peninsula and Britany – Eifel. A negative signal is mostly found inside basins, such as the Ebro and Po Plain. The effect of water extraction in those regions may be the dominant contribution.

At longer time scales, landscape and topography variation can be reconstructed using geological approaches, such as stratigraphy, paleoaltimetry, thermochronology or cosmogenic nuclides to measure rates of exhumation, and geomorphology to interpret uplift rates of dated markers like river or marine terraces. Some regional long-term constraints on the rate of topography variations will be discussed below in the regional context, but we leave a more extensive discussion of geological uplift rates for later work.

2.2. Residual topography

Residual topography is here, and commonly, defined to be the component of topography that is left after subtraction of the isostatic component of the lithosphere from the actual topography. For all topographic signals we shall ignore the elastic flexure contribution by considering wavelengths larger than multiples of the assumed elastic thickness. Here, we use a 250 km width Gaussian smoother for long-wavelength filtering before analysis (e.g. Becker et al., 2014).

To estimate the residual (isostatically anomalous) topography, we need accurate knowledge of the lithospheric structure in terms of density and structure, including the depth of the Moho and the lithospheric thickness, or lithosphere-asthenosphere “boundary” (LAB), and the density distribution within the crustal and mantle parts of the lithosphere. In general terms, the elevation of a lithospheric column with respect to a reference elevation (H), usually taken as the average mid-oceanic ridge elevation, is given by the lithospheric buoyancy, with components from the crustal layer with a thickness (l_c) and density (ρ_c) and the mantle lithosphere with a thickness (l_m) and density (ρ_m), floating over an asthenosphere of density (ρ_a).

$$z_{iso} = (f_1 l_c + f_2 l_m) - H \quad (1)$$

where $f_1 = (\rho_a - \rho_c)/\rho_a$ and $f_2 = (\rho_a - \rho_m)/\rho_a$. Given that f_1 is of the order of 0.1 and f_2 of the order of 0.01, crustal thickness variations thus produce a larger topography signal than the mantle variations; 1 km of crustal change or 10 km of lithosphere mantle change both produce topography change of order of 100 m. Eq. (1) holds for topography under air, the right hand side has to be multiplied by $f_w = \rho_a/(\rho_a - \rho_w) \sim 1.45$ for oceanic regions with water density ρ_w (e.g. Lachenbruch and Morgan, 1990).

Uncertainties in those parameters and hence residual topography estimate may be large and depend on the density distribution, thickness of the lithosphere, and the Moho temperature (e.g. Lachenbruch and Morgan, 1990; Guerri et al., 2015; Gvirtzman et al., 2016). The resolution of crustal thickness is of the order of ± 2 km particularly when considering large regions (e.g. Waldhauser et al., 1998; Spada et al., 2013; Torne et al., 2015; Guerri et al., 2015; Globig et al., 2016; Diaferia et al., 2019). Similarly, deriving crustal density from seismic velocities has a wide scatter and the contributions of temperature variations and other factors are poorly constrained (e.g. Guerri et al., 2015; Gvirtzman et al., 2016). However, most probably, the largest source of uncertainties arises from lithosphere mantle thickness and density variations (e.g. Steinberger, 2016). Here, we therefore focus on crustal corrections to residual topography only, and remove the lithosphere from the contribution to dynamic topography entirely to be broadly consistent in the approach (cf. Panasyuk and Hager, 2000).

Fig. 3a and b show estimates of residual topography in the

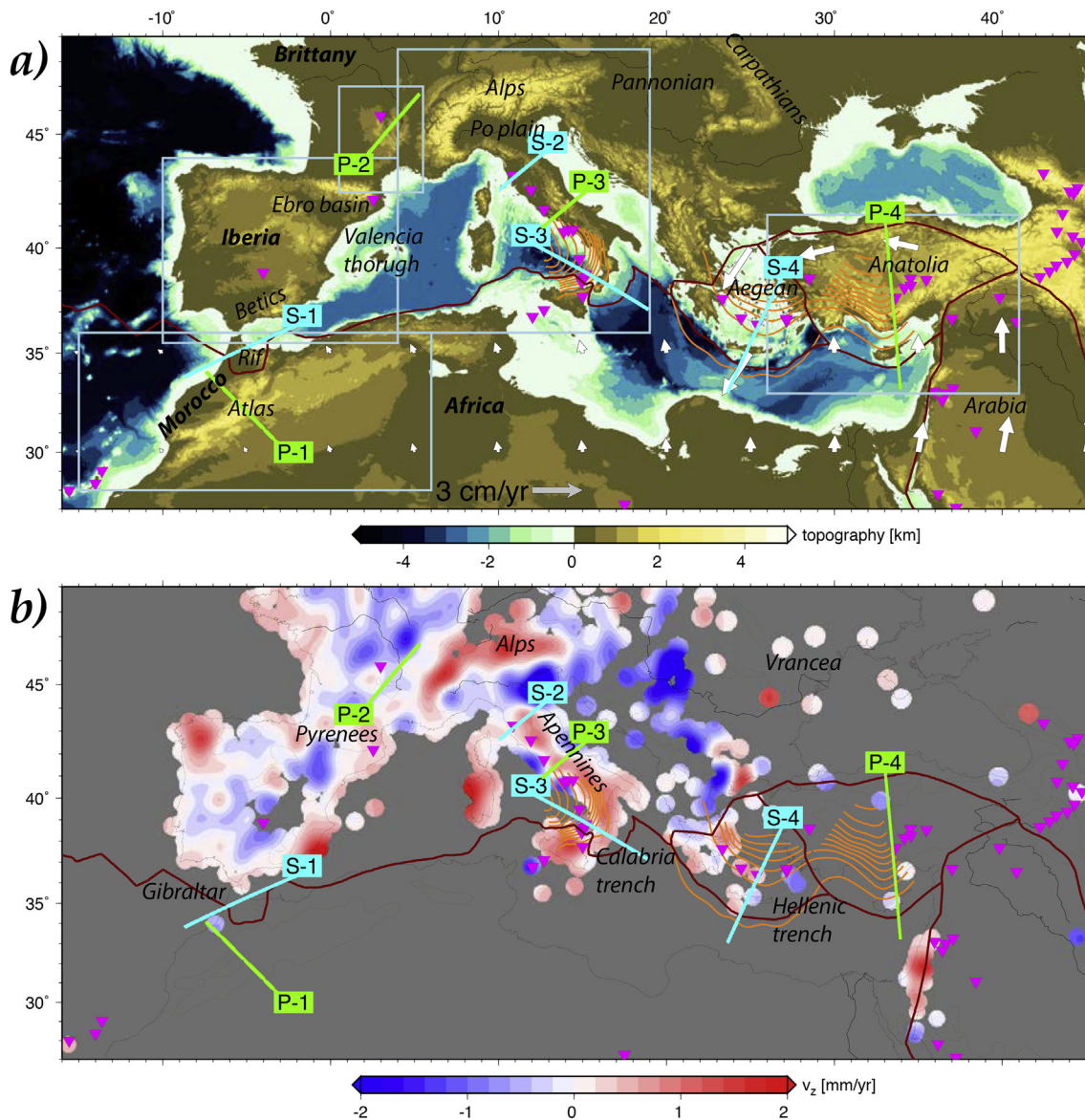


Fig. 2. a) Study region with light blue boxes and profiles showing tectonic settings and margins that are discussed in more detail. This plot and subsequent overview figures show plate boundaries from Bird (2003), recently active volcanism from the Global Volcanism Project (inverted magenta triangles), and slab seismicity contours in 40 km depth contour spacing from SLAB2 (Hayes, 2018); Profiles shown in Figs. 9 and 10 are indicated for subduction (S) and plume/slab detachment (P) settings. White vectors are plate velocities from MORVEL (DeMets et al., 2010), in a Eurasia fixed reference frame. b) Long-wavelength filtered vertical geodetic velocity field, corrected for GIA ICE - 6G model (Peltier, 2004), after removal of a regional mean. GPS vertical velocity field from Serpelloni et al. (2013). Contours of smoothed topography shown at 1 km intervals. (For interpretation of the references to colour in this figure legend, the reader is referred to the web version of this article.)

Mediterranean; these are obtained by correcting oceanic regions for “air-loading” by $1/f_w$ and then subtracting the estimates of eq. (1). Crustal thickness is based on an update of the CRUST1 (Laske et al., 2013) crustal thickness model. This update includes receiver function estimates from Iberia and Morocco (Diaz et al., 2016; Abgarmi et al., 2017), Anatolia – Greece and Middle East (Tezel et al., 2013; Vanacore et al., 2013; Gvirtzman et al., 2016) and from the Alps-Apennines (Piana Agostinetti and Amato, 2009; Piana Agostinetti et al., 2009; Miller and Piana Agostinetti, 2012) but also scattered data from other regions (Molinari and Morelli, 2011). We also allow for (relatively long wavelength) variations in crustal density based on CRUST1 (Fig. 3b). Given the poor knowledge of the lithosphere, in those models, we set thickness of the lithosphere and the density contrast with asthenosphere to constant values that are optimized by minimizing the residual (cf. Becker et al., 2014). This estimate then is one way of assessing

where topography is not in line with crustal thickness variations, but treats contributions from half-space cooling or regions where the mantle lithosphere has been removed, for example, as dynamic (cf. Panasyuk and Hager, 2000).

Results from this approach of estimating “anomalous” topography show a positive signal over most of the backarc regions, the entire western Mediterranean, with exception of the Rif in Morocco, and the Pannonian, Aegean Sea and Anatolia. More to the point, pronounced peaks of residual topography are found in the Atlas, Massif Central, and Galicia. Peaks of positive residuals are often found in places with recently active volcanism, consistent with an interpretation of a deeper, mantle driver (cf. Becker et al., 2014). Negative residuals are found in the Adria plate-Po Plain, Ionian Sea around the Calabria and Hellenic trench and the Rif.

Conversion of free air anomalies can also be used to infer

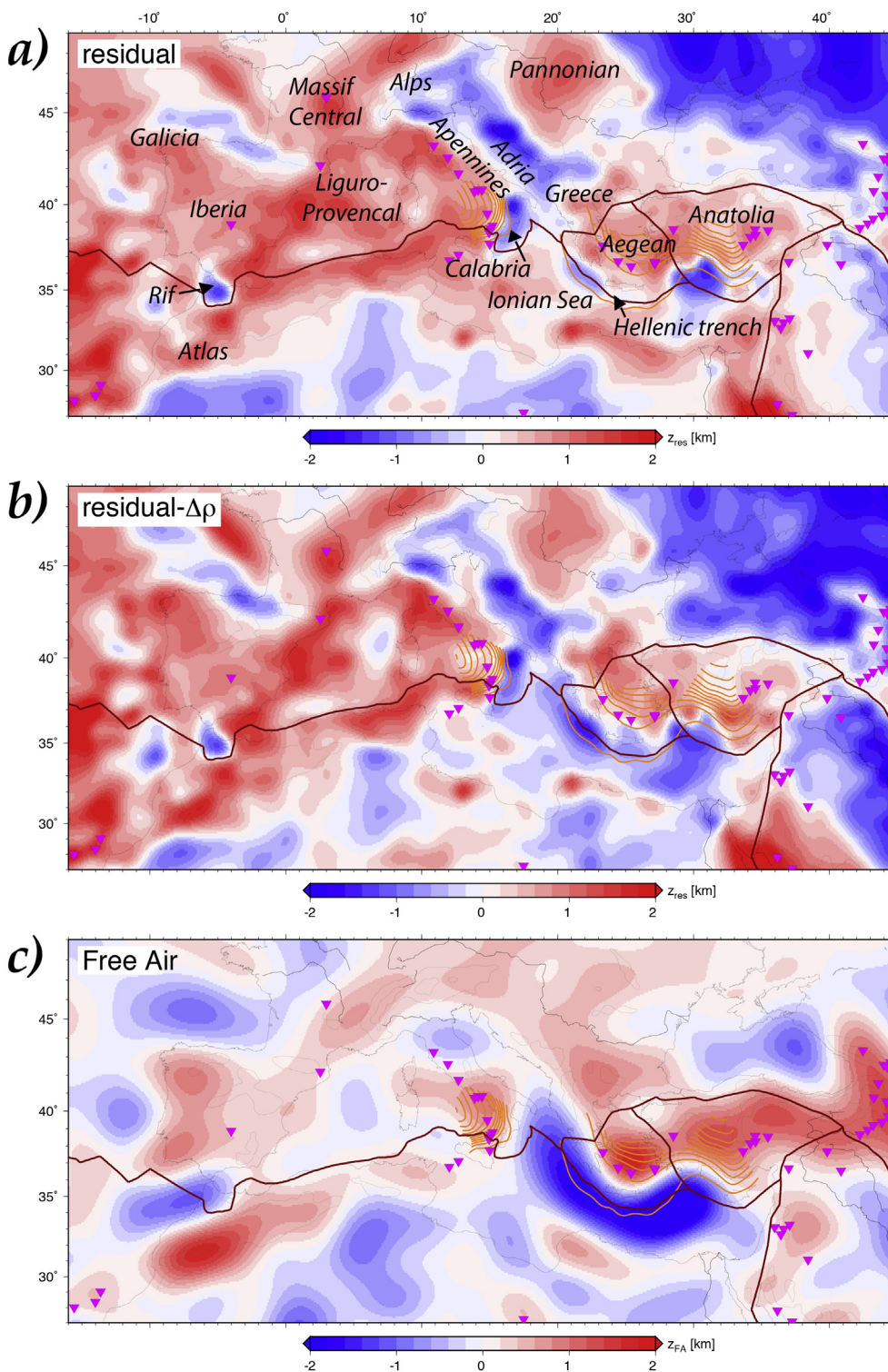


Fig. 3. Estimates of the residual topography obtained by subtracting Airy compensated models of crustal structure from the observed (long wavelength smoothed) topography. Crustal thickness is from an updated merger of regional datasets and CRUST1 and constant crustal density (a), and crustal density variation from CRUST1 (b). Density values used for the crust, lithosphere (constant thickness of 115 km), and asthenosphere are 2781 kg/m³, 3300 kg/m³, and 3226 kg/m³ respectively, the latter optimized by minimizing the residual. c) Non-compensated (“dynamic”) topography estimated from filtered free air gravity anomalies using a constant admittance scaling as in Craig et al. (2011). Inverted magenta triangles indicate recently active volcanism from the Global Volcanism Project. (For interpretation of the references to colour in this figure legend, the reader is referred to the web version of this article.)

“dynamic”, i.e. uncompensated, topography by scaling the gravity anomalies with an “admittance” factor. For Fig. 3c, we used 0.02 km/mGal within an intermediate wavelength range following the choices of Craig et al. (2011) to infer admittance-based anomalous topography. The use of the free air gravity conversion has the advantage to not be explicitly dependent on the choice of crustal and lithospheric mantle structure. However, admittance is not constant in a realistic Earth with depth-variable viscosity (Richards and Hager, 1989; Colli et al., 2016; Yang and Gurnis, 2016), and this approach is in general only a first guess.

We show the free air inferred dynamic anomaly here nonetheless for the sake of argument; Fig. 3c can be compared to Molnar et al.’s (2015) Fig. 5, for example. The case of the Mediterranean has been used to state that amplitudes of residual topography cannot exceed 300 m (Molnar et al., 2015). In fact, the residual topography in the Mediterranean exceeds this value even when inferred from freeair anomalies using the same conversion as in Craig et al. (2011); large portions fall between 500 and 1000 m of residual topography, up to more than 1 km for the Atlas of Morocco, Aegean Sea, and the Anatolia plateau (Fig. 3c).

Regardless of the approach, be it crustal model or gravity anomaly

based, we therefore find that the Mediterranean likely exhibits anomalous topography that is likely not due to simple crustal isostatic balance. The detailed patterns and amplitude are dependent on the corrections that are used, of course, as noted, and these uncertainties are well known (see, e.g., discussion in Faccenna et al., 2014a, for the region). Moreover, the distribution of the topography anomalies shows overall consistency across models (Fig. 3). For example, positive residual topography anomalies emerge in Iberia, the Atlas, the Central Apennines/Tyrrhenian Sea, Anatolia, the Aegean Sea, the Massif Central, the Pannonian and Jordan. Negative residual topography anomalies are found over Gibraltar, Northern Apennines, the Ionian Sea, and the Black Sea. Within the oceanic domain, half-space cooling and subduction are clear drivers of such signals, but their origin within the continental or transitional domains is less clear and will now be explored further.

2.3. Dynamic topography

Here, dynamic topography is defined as the deflection of the surface of the Earth due to active mantle flow (e.g. Ricard et al., 1984; Panasyuk and Hager, 2000). To first order, this deflection of the surface scales with the normal stresses that would be induced by convective mantle flow at a vertically fixed surface. For a given density anomaly, those stresses depend on the distance from the interface, for example, and viscous stress amplitudes scale as strain-rate times viscosity, by definition. Strain-rates depend on gradients of velocity, and those velocities themselves scale with density anomaly divided by viscosity (as for the Stokes sinker case). Dynamic topography thus scales linearly with the driving mantle density anomalies to first order (e.g. Hager et al., 1985; Gurnis et al., 2000) and viscosity variations are of secondary relevance. Topography change over time, i.e. uplift, is expected to scale as topography times velocity, thus as density anomaly squared over viscosity. Both dynamic topography and uplift are thus dependent on the asthenospheric density anomaly, as inferred, e.g., from seismic tomography, but viscosity mainly comes mainly into play for uplift rates (e.g. Hager et al., 1985; Gurnis et al., 2000). In practice, density anomalies in the uppermost mantle are most relevant (e.g. Richards and Hager, 1989), and lateral viscosity variations will serve to modulate the topographic expression of anomalies, though not affect the overall scaling to first order.

At global or continent scales (> 500 km), much progress has been made in the understanding of dynamic topography. For example, large-scale tilting of continental interiors has been modeled and calibrated by the stratigraphic record of marine inundations or by uplift of marine terraces (e.g., Gurnis, 1993; Lithgow-Bertelloni and Gurnis, 1997; Lithgow-Bertelloni and Silver, 1998; Forte, 2000; Gurnis et al., 2000; Liu et al., 2008; Moucha et al., 2008, Moucha and Forte, 2011; Shephard et al., 2010; Flament et al., 2013, 2015; Rowley et al., 2013a, Rowley et al., 2013b; Forte et al., 2009; Forte et al., 2010; Müller et al., 2018).

The field is progressing rapidly with increased computational capabilities and higher resolution seismic velocity models leading to better estimates of topography change. However, a number of questions remain debated, including the role of lithosphere strength and layering on transmitting deep signals to the surface and the amplitude and rates of the process, which strongly depend on poorly constrained density and viscosity parameters (Morgan, 1965; Burov and Gerya, 2014; Becker et al., 2014; Kiraly et al., 2015; Sembroni et al., 2017; Hoggart et al., 2016; Steinberger, 2007, 2016; Davies et al., 2019; Steinberger et al., 2019).

To model dynamic topography due to asthenospheric density anomalies (e.g. Becker et al., 2014), we need to start out with a well-resolved tomography model before assessing the role of plate boundaries and other lateral viscosity variations. Fig. 4 shows results from three different tomographic models illustrating dynamic topography based on the global shear wave models SAVANI (Auer et al., 2014),

TX2015 (S. Grand, pers. comm.), and a combination of the regional model M01 (Piromallo and Morelli, 2003) and TX2015. The mantle flow computations are purposefully simple and use with the spectral code HC (cf. Milner et al., 2009), using only radially variable viscosity with all general parameters and assumptions as in Faccenna et al. (2014a), Faccenna et al., 2014b); see there for details. Globally, the mantle flow that results from these assumptions, e.g. as to scaling between density and shear wave velocity anomalies, $d\ln v/d\ln \rho = 0.18$, is broadly consistent with plate velocities and geoid anomalies (e.g. Ghosh et al., 2013). The scaling is applied to all tomography anomalies below 100 km, above of which it is set to zero. Dynamic topography in Fig. 4 shown as air loaded.

The dynamic topography model shows a positive signal mostly over the large basins, e.g. eastern Iberia -Liguro-Provençal, and the Pannonian and Aegean backarc basin, the Tyrrhenian and central-southern Apennines, but also Eastern Turkey and the Sicily channel. Positive dynamic topography over arcs may be expected due to the presence of a low seismic velocity anomaly. In some cases, those velocity anomalies may be in part due to partial melting, and this is one example where the conversion of tomographic velocity anomalies to temperature is likely oversimplified. Negative anomalies in topography are mostly found over active subduction zones.

Comparing residual and dynamic topography can help to identify mantle-driven signals (e.g. Becker et al., 2014), but uncertainties on both residual and dynamic topography estimates may still be significant (e.g. Lachenbruch and Morgan, 1990; Steinberger, 2007; Guerri et al., 2015; Steinberger, 2016). Comparing the dynamic estimates from the two global models in Fig. 4, they are broadly consistent on large scales visually, and the spectral character is comparable at modest correlation (see supplementary material). However, some of the differences between residual and dynamic topography are of the same spatial scale as regional features, and this difference may be used to understand the origin of the anomalies.

Using a regional tomography model (Fig. 4c) clearly enhances the smaller-scale signal on the surface, as expected given the linear scaling between density anomaly and dynamic topography, and such regional high-resolution seismic models are likely required for many tectonics applications. While the M01 model that is used for Fig. 4c is likely not the last word on Mediterranean structure, it has been explored widely (e.g. Boschi et al., 2010), and serves as our best regional estimate here.

To understand the link to tectonics, it is crucial to focus the analysis on regional scales (cf. Steinberger, 2016), and to further compare the individually relatively uncertain residual and dynamic topography signals with geodetic, geomorphological and geological studies documenting recent to active vertical surface motion, which we will do next.

3. Topography of Mediterranean region

Mantle downwellings and upwellings have apparent links to distinct topographic features that are presented here with case studies extracted from the Mediterranean region.

3.1. Subduction and orogeny related topography

Mantle downwelling and upwellings produce distinctive topographic features. In subduction and collisional systems, both isostatic and dynamic contributions are expected to be pronouncedly different from average global values (e.g., Lachenbruch and Morgan, 1990). The isostatic contribution at convergent margins matters as tectonic deformation of the upper plate produces variations of crustal thickness. Dynamically, stresses associated with the negative buoyancy of the dense slab are transmitted up into both the forearc of the overlying plate and the foreland on the subducting plate (e.g. Karner and Watts, 1983; Royden, 1993; Royden and Husson, 2006; Zhong and Gurnis, 1994). This produces surface depressions, but changes in the slab load

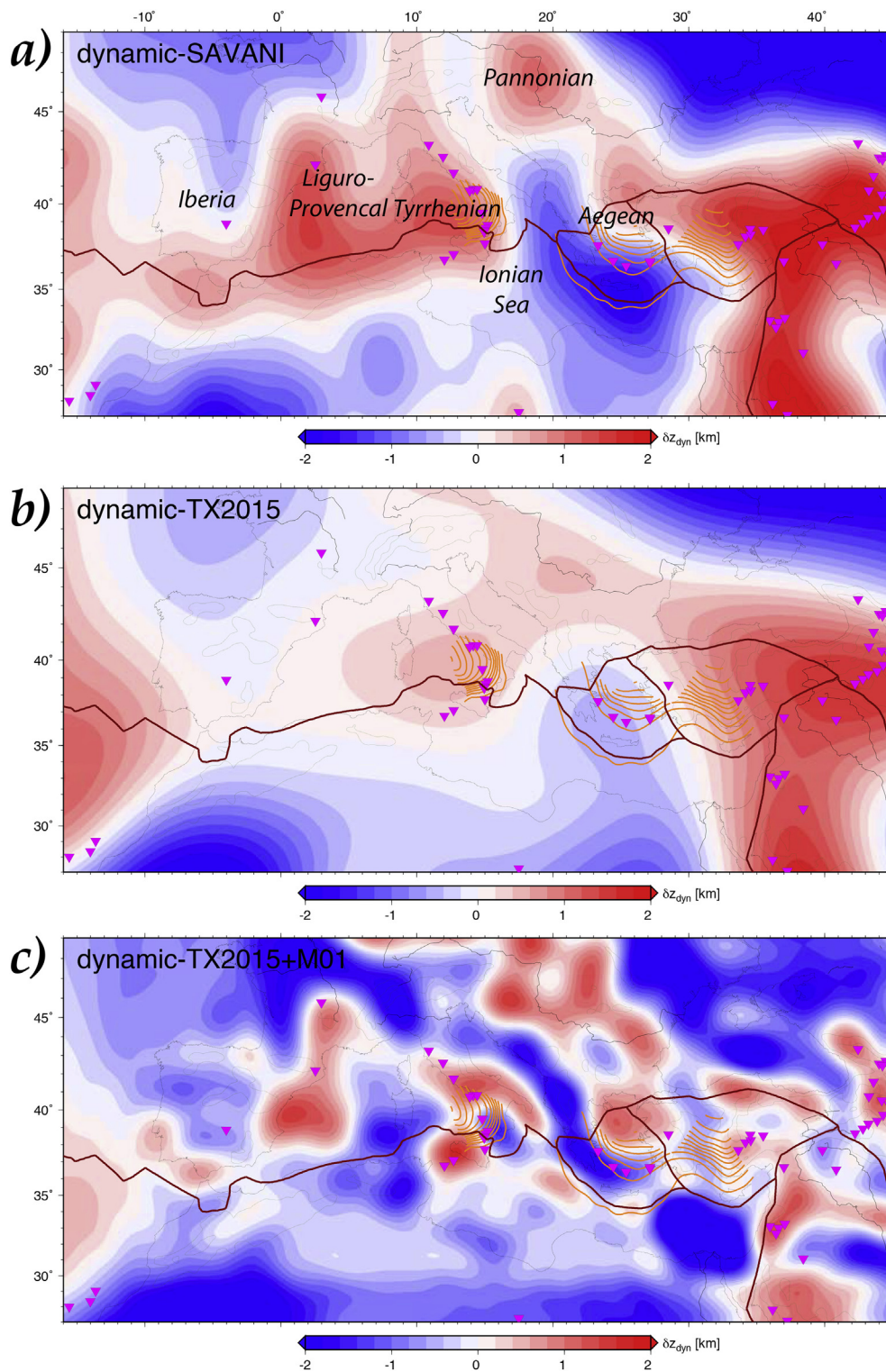


Fig. 4. Predictions of dynamic topography from inferred surface deflections as caused by present-day mantle flow. a) Using the SAVANI model of Auer et al. (2014); b) the global S wave model TX2015 by S. Grand (pers. comm., 06/2018) and, c), M01 (Piomallo and Morelli, 2003) embedded in TX2015.

or geometry can then lead to uplift or subsidence of the overlying regions. Subduction also induces the mantle flow pulling down the upper plate introducing a larger-scale negative dynamic topography (e.g. Mitrovica et al., 1989a; Mitrovica et al., 1989b; Zhong and Gurnis, 1994; Cramer et al., 2017). In particular, the amplitude of the dynamic topography increases with slab pull during trench roll-back and slab shallowing as the negative density anomaly moves relatively closer to the surface (Mitrovica and Jarvis, 1985; Mitrovica et al., 1989a, 1989;

Cramer et al., 2017). Variations of those parameters are expected to produce negative or positive temporal change in topography (uplift and subsidence in location fixed relative to the slab trajectory), while the overall dynamic topography is negative. The reaction to this load is expressed during slab break-off which produces uplift (Wortel and Spakman, 2000; Regard et al., 2008; Duretz and Gerya, 2013; Duretz et al., 2014; Garzanti et al., 2018). We note that this recovery of topography after break off is not elastic rebound, but simply due to

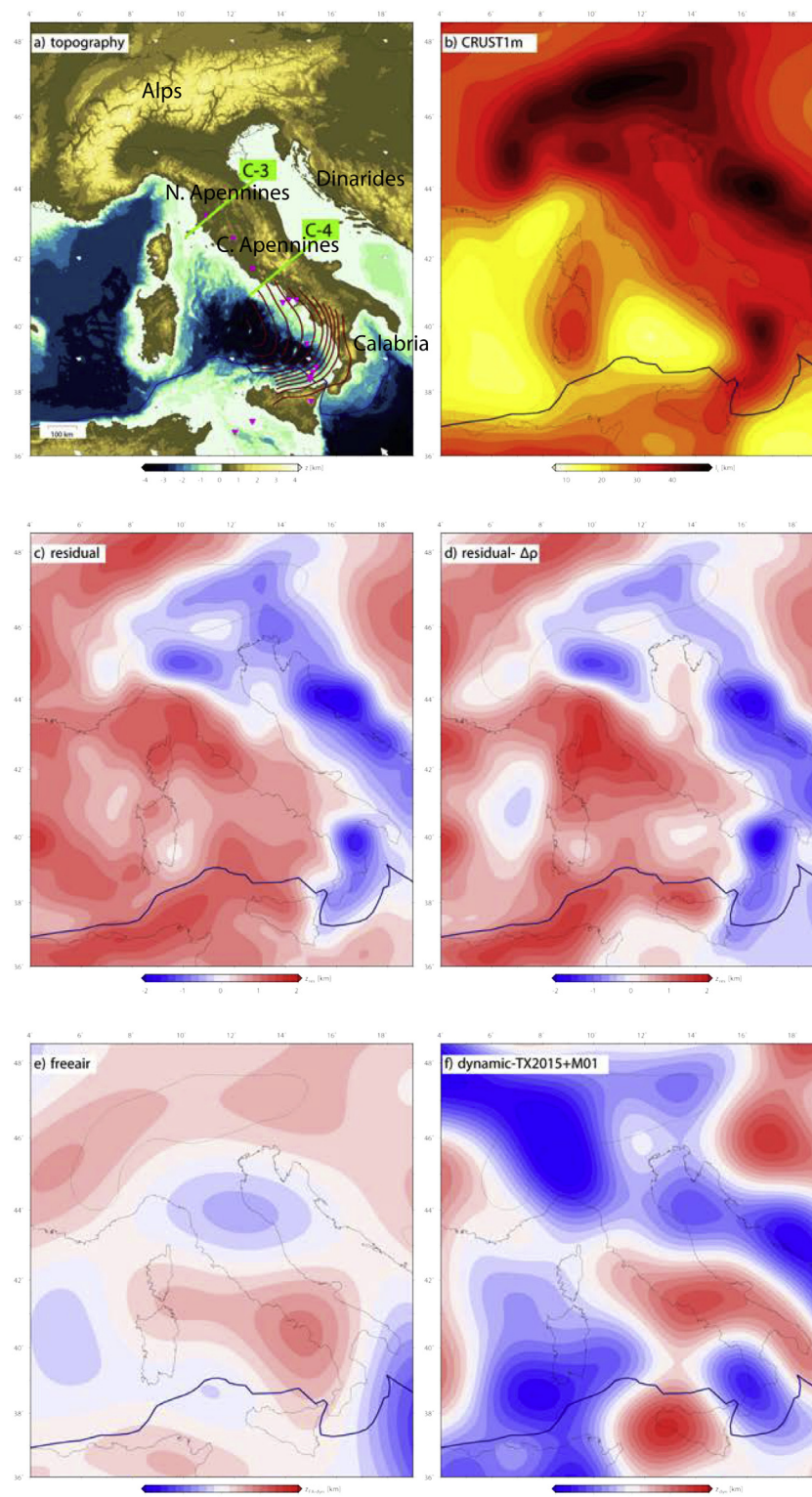


Fig. 5. Central Mediterranean topography (a). Crustal thickness is from an updated merger of regional datasets and CRUST1 (b) used to estimate residual topography using constant density (c) or with crustal density variation from CRUST1 (d) (as in Fig. 3a and b). Dynamic (non-compensated) topography estimated from filtered free air gravity anomalies using the “admittance” scaling as in Craig et al. (2011) (e, as in Fig. 3c) and dynamic topography as in Fig. 4c.

successive reductive of the negative dynamic topography in a purely viscous system.

The entrance of the slab into the lower mantle is also expected to induce an even longer wavelength, low amplitude negative signal (e.g., Pysklywec and Mitrovica, 1997; Pysklywec and Mitrovica, 1998). Because of the larger depth scales involved, the horizontal spatial

expression is increased as well, albeit at lower amplitude because of the distance between the surface and the density anomaly. At convergent margins, those fluid slab sinker effects should be superimposed on the shallow flexural signal of foredeep basins (e.g., Davila et al., 2010; Flament et al., 2015) and bending of the lithosphere at the trench can produce depression due to flexural isostasy (Karner and Watts, 1983).

In the following, we will discuss some examples of subduction zone signals from the Mediterranean. In a subduction context, and more generally, residual and dynamic topography do not have to necessarily match, as usually assumed. They may reveal processes occurring at different depths, with the shallow (mantle or sub-mantle lithosphere convection) signal better expressed by residual topography and the deeper mantle signal better expressed by dynamic topography. The uplift rate depends likewise on the competition between those processes. Moreover, uplift patterns do not necessarily have to match the residual or dynamic topography signal, as there may well be uplift over regions with negative residual/dynamic topography, for example in the case of rebound after slab break off.

In the Mediterranean, subduction zones have reached a late stage of evolution as active Wadati-Benioff zones are only found below the Hellenic and Calabrian trenches (Fig. 2). Intermediate to deep (~50 to 500 km), discontinuous seismicity is found below the Vrancea Zone, Gibraltar, and the Northern Apennines implying a once longer and wider subduction system (e.g., Royden and Faccenna, 2018). Other convergent margins are in a collisional stage, i.e. where the slab is partly or totally broken off (Wortel and Spakman, 2000), their activity has vanished, as in the Pyrenees, or is partially active in some specific place, such as on the foothills of the eastern Alps (Fig. 2).

The different regional topographic signals of convergent margins can be compared to obtain information about different temporal stages of continental collision, progressing from: a), subduction of oceanic lithosphere, to, b), subduction of continental lithosphere, and, lastly, c), collision and slab break.

The Alps-Apennines. The Apennines-Alps is a key site to analyze the vertical motion during those three distinctive collisional stages. The Apennines orogen formed mostly during the Neogene (Malinverno and Ryan, 1986; Patacca et al., 1990; Royden, 1993; Carminati and Doglioni, 2012; Carminati et al., 2012; van Hinsbergen et al., 2014; Royden and Faccenna, 2018), piling up slices of continental margin material scraped off from the subducting Adria lithosphere (e.g., Patacca et al., 1990). The Alps were formed earlier mostly in the Early Tertiary, during the closure of small oceanic basins, and evolving into a collisional stage between Adria and Eurasia sometime during the Oligocene (e.g., Carminati and Doglioni, 2012).

Stage a) of oceanic subduction is currently active below Calabria; stage b), continental subduction, is active in the northern Apennines; and, c), the Central Apennines subduction appears in the recent stage of slab breakoff (e.g. Wortel and Spakman, 2000; Faccenna et al., 2014b). The Alps are in an advanced stage of collision, as subduction vanished some tens of millions of years ago (e.g. Sternai et al., 2019).

The Calabria subduction zone is representative of stage a) with subduction of the Ionian ocean beneath Eurasia. It shows the presence of an active arc, the Aeolian Islands, a forearc high onshore Calabria, cross-cut by active normal faults and quickly uplifting, and a very shallow angle taper accretionary wedge in the Ionian Sea (e.g., Doglioni et al., 1999; Minelli and Faccenna, 2010). The backarc area of the Calabria subduction zone is represented by the Tyrrhenian Sea, which is locally floored with oceanic crust and was extended in the last ~12 Ma (Sartori, 1990). Comparison of geological with geodetic constraints indicates that Tyrrhenian extension vanished sometime during the Late Pleistocene (D'Agostino and Selvaggi, 2004).

The residual and dynamic topography signals for Calabria are negative (Fig. 5). Marine terraces indicate that the onset of uplift started in the Lower Pleistocene at rate of ~0.8–1 mm/yr (Ferranti et al., 2006; Faccenna et al., 2011; Olivetti et al., 2012). As discussed below, this may be related to active crustal thickening (i.e., Minelli and Faccenna, 2010), a decrease in the sub-lithospheric load, e.g. slab break-off, or shallower toroidal flow (Faccenna et al., 2011). In the Tyrrhenian backarc, residual topography is positive, while dynamic topography is slightly negative, besides over the Central Apennines and Sicily (Fig. 5). The presence of the pair of negative residual topography at the trench and positive anomaly in the backarc region is also observed in the other

active Mediterranean subduction zones, such as the Hellenic, Pannonian or Alboran (Fig. 3). In the Hellenic trench we also notice that the residual topography estimates from free air gravity anomaly provide an unrealistically high positive value of more than 1 km in the Cretan Sea.

The northern Apennines is a remarkable example of stage b) of continental subduction. The northern Apennines belt is an active, low-taper accretionary wedge, with active compression in the front and extension on the mountain crest, with mean elevation of ~300–400 m (estimated along a 100 km wide swath profile, Figs. 3 and 10). It is a subduction orogen, growing during continental subduction by scraping off and transferring material from the subducting plate to the upper plate (e.g., Carminati and Doglioni, 2012; Piana Agostinetti and Faccenna et al., 2018; Royden and Faccenna, 2018) and the divide is located in correspondence of the plate contact at depth (e.g., Piana Agostinetti and Faccenna, 2018). Like other subduction settings, the northern Apennines also show a slightly negative residual topography of ~200/–300 m, with relevant crustal thickness of up to 50 km floating over hot asthenosphere (e.g., Panza et al., 2007; Di Stefano et al., 2011; Piana Agostinetti and Faccenna, 2018), turning into a positive anomaly toward the backarc region (Fig. 5). The northern Apennines show subsidence on its foredeep side and Po Plain (Carminati and Martinelli, 2002; Carminati et al., 2003). Similar to the Northern Apennines, the Peloponnese to the Dinarides, for example, on the other side of the Adriatic, there is also negative to zero residual topography.

The Central Apennines represents a recent case of slab break-off. The presence of a break in the slab is supported by the lack of deep seismicity, by the presence a shallow slab gap in seismic tomography and by the lack of shallow compressional seismicity and deformation (Gvirtzman and Nur, 2001; Chiarabba et al., 2005; Lucente et al., 1999; Wortel and Spakman, 2000; Piromallo and Morelli, 2003; Giacomuzzi et al., 2012; Faccenna et al., 2014b).

The Central Apennines stands at higher average elevation, ~600 m, than the Northern Apennines and Calabria, even if its crustal thickness is lower by about ~10 km than that of the Northern Apennines and Calabria (Faccenna et al., 2014b). The highest portion of the central Apennines wedge is under extension, and compression at the front is sealed by Lower Pleistocene deposits (Patacca et al., 1990; D'Agostino et al., 2001; Pizzi, 2003). The central Apennines shows a positive residual topography of ~400 m, and a positive dynamic topography of almost the same amplitude (Fig. 5). Rates of uplift here as from geodesy are of the order of 0.2–0.4 mm/yr (Fig. 2c; cf. Faccenna et al., 2014a, Faccenna et al., 2014b).

The Alps represent a more advanced stage in the evolution of a collision zone (e.g., Carminati and Doglioni, 2012). Here, subduction vanished at ~30 Ma, while compression is active only in a small portion of the eastern Alps. The Alps are characterized by fast geodetically determined uplift, up to ~1 mm/yr, faster than elsewhere in the Mediterranean (Serpelloni et al., 2013). The Alps also show only a slightly negative to null residual topography, and negative dynamic topography (cf. Sternai et al., 2019). Conversely to the Apennines case, the Alps thus show topography in good correlation with crustal thickness, suggesting that the isostatic contribution dominates.

3.2. The Atlas

The northwest African margin is crossed by several mountain belts, running from the Atlantic Ocean to the Mediterranean. The Anti-Atlas is to the south of the steeper High Atlas and the orogeny overall stretches WSW-ENE over the whole North Africa margin. The Middle Atlas trends NE-SW and departs from the High Atlas toward the Mediterranean. The Rif in Morocco and the Tell in Algeria are the northernmost belts, running along the Mediterranean coast and turning around Gibraltar (Fig. 6).

The North African relief is generated by shortening and transpression due to Africa and Eurasia convergence. The convergence system

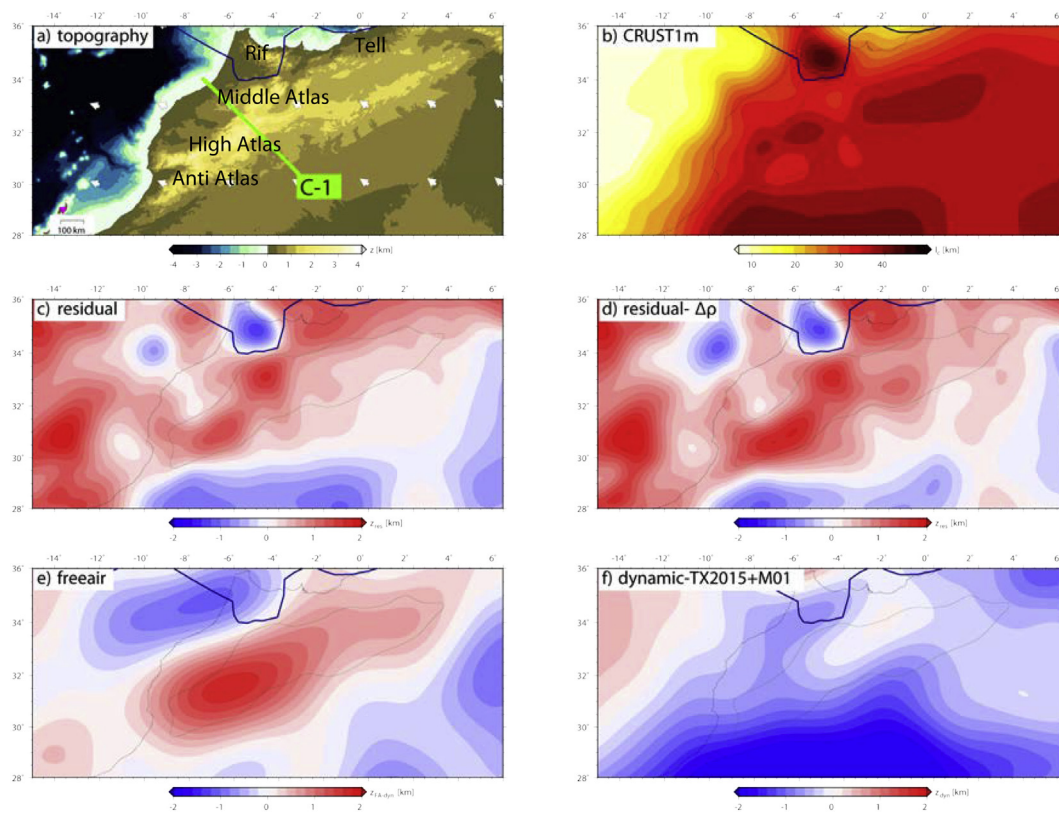


Fig. 6. Atlas topography (a). Crustal thickness is from an updated merger of regional datasets and CRUST1 (b) used to estimate residual topography using constant density (c) or with crustal density variation from CRUST1 (d). Dynamic (non-compensated) topography estimated from filtered free air gravity anomalies using the “admittance” scaling as in Craig et al. (2011) (e) and dynamic topography as in Fig. 4c.

first produced the consumption of the Tethyan Sea and its margins forming the Tell-Rif-Betic system, and then compression shifted southward in the Atlasic system, re-activating pre-existing Mesozoic extensional features. The shape of the belt, in particular that of the High and Middle Atlas, mirrors the trend of the pre-existing rift system (Frizon de Lamotte et al., 2000; Frizon de Lamotte et al., 2011; Gomez et al., 1998; Gomez et al., 2000). The main phase of inversion and the creation of a steep relief in the High Atlas occurred recently, probably during the last 10 Ma or so, after the cessation of subduction in the Mediterranean (Faccenna et al., 2014a, Faccenna et al., 2014b; Tezel et al., 2013). The Atlasic system is thus an intracontinental orogen. Several studies suggest that the elevation and uplift history of the Atlas is attributed to mantle dynamics (Teixell et al., 2003, 2005; Missenard et al., 2006; Miller and Becker, 2014; Duggen et al., 2009; Babault et al., 2008; Miller et al., 2013; Gomez et al., 1998; Sun et al., 2014; Civiero et al., 2018; Lanari et al., 2020).

The High and Middle Atlas reaches an average altitude of more than 1000 m, with relatively thin crustal thickness (Miller and Becker, 2014; Ayarza et al., 2014; less than 40 km; Suppl. Mat. Fig. S2). The resulting residual topography is ~500–800 m. Conversion of free air anomaly also provides a notably positive topography signal of up to ~1500 m. Dynamic topography also shows a positive signal of up to 500–800 m and is related to the presence of a slow shallow positive anomaly located beneath the High Atlas (Sun et al., 2014; Civiero et al., 2018). The Atlas plateau of Algeria is also a weakly deformed, flat region standing at an elevation of more than ~1000 m. The uplift of the Atlas occurred recently, during the last 5 Ma, as attested by Messinian marine deposits standing at elevation of up to ~1200 m a.s.l. (Teixell et al., 2005; Babault et al., 2008).

Moving to the North, in the Rif area, the setting is different; the crust is thicker than in the Atlas (Thurner et al., 2014; Ayarza et al., 2014; Gil et al., 2014; Diaz et al., 2016) but the elevation is lower,

giving a remarkable negative signal on the residual topography (Fig. 6c) while the dynamic topography is slightly positive. In the Alboran Sea backarc region the residual topography signal is positive. This trend resembles that of the other subduction settings, for example the Calabria and Hellenic sections (Fig. 3b).

The Anatolian orogenic plateau. Anatolia is an orogenic plateau formed during Tethyan closure by episodes of collision and accretion of continental slivers (Sengor et al., 2003). It stands at an elevation of ~2 km and it is bounded by the North Anatolian fault to the North, by Cyprus subduction and East Anatolia Faults to the South, by the Aegean extensional domain to the West and by the Bitlis-Caucasus collisional zone to the East. Most tectonic processes, including the Aegean extension, North Anatolia Fault formation and Arabia-Eurasia collision occurred at the same time, i.e. during the Neogene and are still active today (Sengor et al., 2003; McKenzie, 1976). The possibility that the topography and the rise of the Anatolia plateau has a dynamic origin has been widely debated (Sengor et al., 2003; Faccenna et al., 2006, 2013; Zor et al., 2003; Gogus, and Pysklywec, 2008; Karabolut et al., 2019; Bartol and Govers, 2014; Komut et al., 2012; Göğüş et al., 2017).

The thickness of the Anatolia plateau crust decreases westward moving from the collision zone, decreasing from up to 50 km to 20 km or less to the Aegean extensional province. The Central Anatolia Plateau has a thickness of ~35–40 km (Fig. 7; Vanacore et al., 2013; Karabolut et al., 2019). Overall, crustal thickness matches the topography (e.g., Karabolut et al., 2019; with a large scatter around ~30–35 km).

Residual topography is positive at ~500–600 m on the Taurides and on southwest Turkey. Conversion of free air gravity anomaly shows very high value of more than ~1200 m of residual topography over Anatolia, increasing in Greece to more than ~1800 m. Dynamic topography overall shows negative values, except in the Taurides – Cappadocia (Central Anatolia Plateau) (Fig. 7f). Sedimentary deposits and incision rates indicate rapid uplift in the Taurides, with Upper

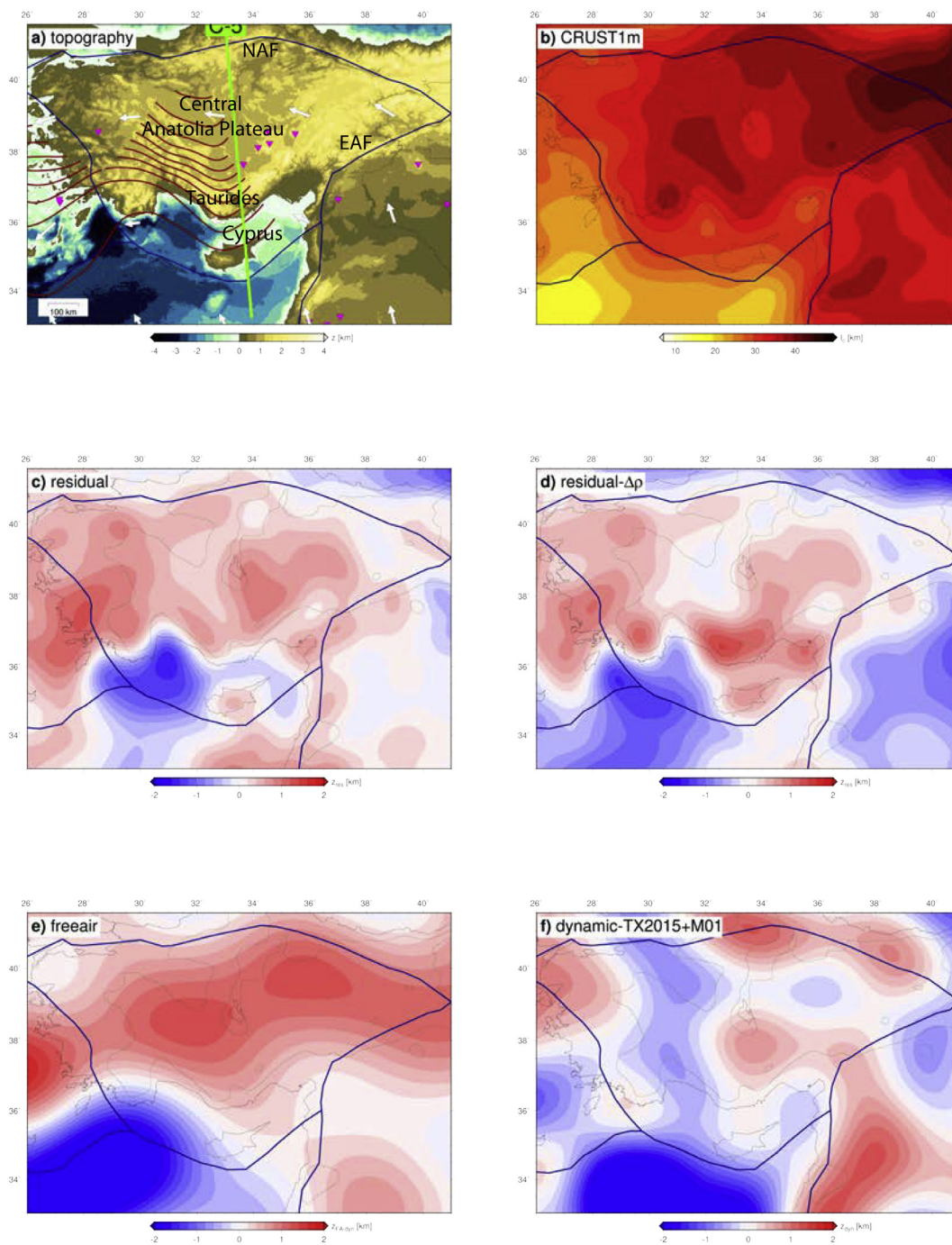


Fig. 7. Anatolian topography (a). Crustal thickness is from an updated merger of regional datasets and CRUST1 (b) used to estimate residual topography using constant density (c) or with crustal density variation from CRUST1 (d). Dynamic (non-compensated) topography estimated from filtered free air gravity anomalies using the “admittance” scaling as in [Craig et al. \(2011\)](#) (e) and dynamic topography as in [Fig. 4c](#). NAF indicates North Anatolia Fault, and EAF indicates East Anatolia Fault.

Miocene to Early Pleistocene marine sediments (~ 1.6 Ma) cropping out at ~ 2 km and ~ 1.2 km elevation, respectively, yielding variable but relatively fast uplift rates ([Cosentino et al., 2012](#); [Schildgen et al., 2014](#); [Öğretmen et al., 2018](#)). The uplift history of the central Anatolia Plateau is more uncertain and stable isotopes shows that most of the plateau uplift, more than ~ 1300 m, occurred from ~ 11 to ~ 5 Ma during an ignimbrite flare up ([Meijers et al., 2018](#); but overall lower rates compared to the Taurides ([Schildgen et al., 2014](#)).

3.3. Intraplate topography and localized mantle upwelling

Mantle upwellings may be related to return flow, for example within the backarc (e.g., [Faccenna et al., 2011](#)), or to positively buoyant mantle plumes. The topographic signal over plumes has been widely investigated at many scales (e.g. [Morgan, 1965](#); [Ribe and Christensen, 1994](#); [Griffiths et al., 1989](#); [Steinberger et al., 2001](#); [Burov and Cloetingh, 2009](#); [Burov and Guillou-Frotier, 2005](#); [Burov and Gerya, 2014](#)). Upwelling of buoyant material is expected to produce upwarping of the lithosphere and hence a positive residual and dynamic signal. However, depending on the structure of the lithosphere, the

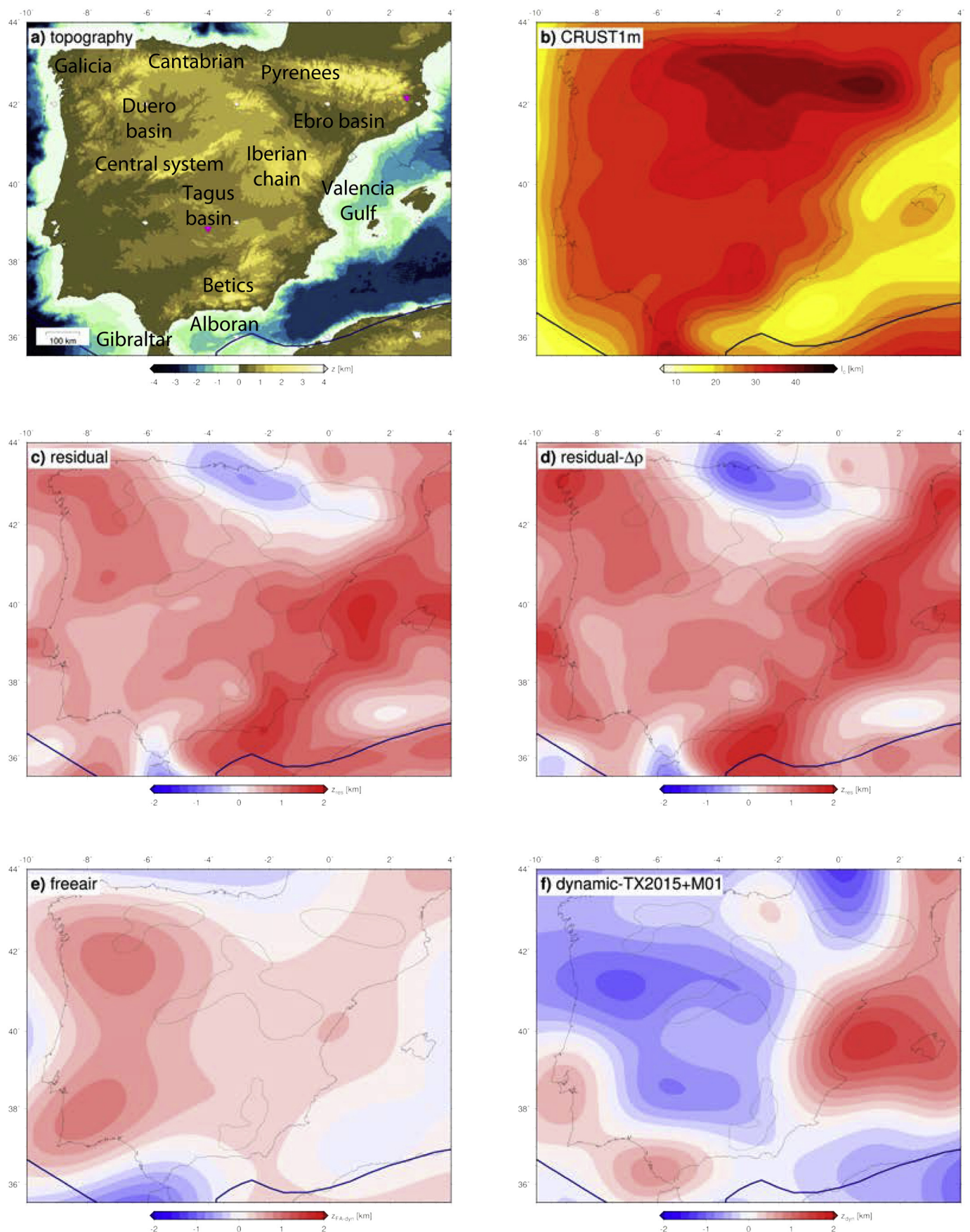


Fig. 8. Iberia topography (a). Crustal thickness is from an updated merger of regional datasets and CRUST1 (b) used to estimate residual topography using constant density (c) or with crustal density variation from CRUST1 (d). Dynamic (non-compensated) topography estimated from filtered free air gravity anomalies using the “admittance” scaling as in Craig et al. (2011) (e) and dynamic topography as in Fig. 4c.

resulting topography signal may be different. For example, return flow from the upwelling mantle could induce a lateral dripping of the mantle lithosphere, inducing first subsidence but then uplift (Burov and Gerya, 2014). The lithospheric structure itself affects the size and amplitude of the bulge (e.g. Morgan, 1965; Griffiths et al., 1989; Sembroni et al., 2017; Bodur and Rey, 2019), and the possibility for the lower crust to flow outside the bulge can also contribute to smooth out the expected topographic bulge (Burov and Gerya, 2015; Sembroni et al., 2017).

Small, “baby”, upper mantle plumes have been described below Europe, in particular in the Eifel, Massif Central, and Bohemian massif volcanic field (e.g. Hoernle et al., 1995; Goes et al., 1999; Sobolev et al., 1997). Those plumes are expressed by sustained volcanism and topographic doming at the surface, and several have been well imaged by high resolution tomography (e.g., Ritter et al., 2001). Volcanism in both Eifel and the Massif Central was long lasting over the Tertiary. For the Eifel, a joint seismic and geodynamic approach suggests a $\sim 60\text{--}80$ km radius plume with approximately 200°C excess temperature (Wüßner et al., 2006). Uplift history derived from ~ 800 kyr from river incision reveals a concentric pattern uplift of up to ~ 250 m extended over a region of ~ 200 km, with a peak surface uplift rate of ~ 0.3 mm/yr (Meyer and Stets, 1998; Garcia-Castellanos et al., 2000). The Black Forest plateau is probably similar, but shows a very slow rate of rock uplift related to surface uplift of ~ 400 m that started probably ~ 19 Ma (Meyer et al., 2010).

The Massif Central is characterized by high heat flow (up to ~ 100 mW/m²) (Lucazeau et al., 1984), negative Bouguer gravity anomalies (up to -70 mGal) (Sobolev et al., 1997) and a thin/normal crustal thickness of ~ 25 km (Tesauro et al., 2005). A low-velocity zone of seismic waves has been imaged between 30 and 250 km from local seismic tomography (Granet et al., 1995), while large-scale tomographic models extend this low-velocity anomaly to ~ 300 km and more. Olivetti et al. (2016) Lower Pliocene marine deposits standing at an elevation of ~ 200 m a.s.l. provides an average surface uplift at rates of ~ 0.06 mm/yr (Olivetti et al., 2016), similar to the exhumation rate (Olivetti et al., 2020) Residual topography in the Massif Central is positive of the order of ~ 1000 m or more, and free air gravity converted residual topography is also positive like the dynamic topography is and in the range of $\sim 600\text{--}800$ m (Fig. 3). Volcanism and uplift in the Vogelsberg Mts., Rhine and Bohemian massifs show similarities with those discussed here for the Massif Central.

These small plumes can be compared with the Ethiopian plateau, which represents one of the largest Large Igneous Provinces (LIPs), erupted at $\sim 30\text{--}32$ Ma over the Afar plume (Ebinger and Sleep, 1998). The residual topography for the Ethiopian plateau is ~ 600 m, while the dynamic topography exceeds ~ 1000 m. Reconstruction of the geometry of the lava flow provides constraints on the uplift history (Sembroni et al., 2016). After the lava flood emplacement around 30 Ma we see an increase of the average elevation by ~ 1000 m that ended around 10–12 Ma, prior to the rifting. This gives average rate of 0.05 to 0.1 mm/yr. Modeling also shows a long term, slow dynamically induced surface uplift (Faccenna et al., 2019). Interestingly, during the last 10 Ma, the topography of the Ethiopian plateau remained stable, indicating a long-term dynamic support of the topography lasting for tens of myrs. Hoggard and Tibesti probably had a similar evolution; these topographic features stand over the landscape and produced the first eruption in the Eocene-Oligocene (Rudge et al., 2015; Paul et al., 2014).

The Iberian plate. Iberia was an independent microplate during the opening of the northern Atlantic, separating from North America and travelling westward and then colliding with Eurasia. It is bounded by orogens and extensional basins: the Pyrenees-Cantabrian and Betic orogenic belts to the North and the South, respectively; the Ligurian-Valencia-Alboran and the Atlantic extensional systems to the East and to the West, respectively. In its interior, the plate is deformed by the Central system and the Iberian system and large basins. Overall, orogenic belts trend E-W and follow pre-existing extensional feature. Orogenic phases progressively young to the south: the Pyrenees from

late Eocene to early Oligocene, the Iberian-central system from late Oligocene to Miocene and then the Betic system, mostly active during the Neogene (e.g., Casas-Sainz and Faccenna, 2001). Thrusting and internal faulting created internally drained basins such as the Duero and Ebro to the north and the high Tagus to the south. During the Neogene, those basins started draining into the sea, producing fast erosion and shaping river morphology. River analysis over the entire Iberia peninsula has been used to infer a recent uplift episode (Roberts et al., 2019). Compression and thrusting vanished in the Neogene in Iberia.

The topography of the Iberian peninsula is characterized by high average elevation ($\sim 600\text{--}700$ m) with flat surfaces, mesetas, developed over the Iberia peninsula (Casas-Sainz and De Vicente, 2009). The causes of the elevation have been debated and models suggest that the relief has been produced by long wavelength lithosphere folding (Cloetingh et al., 2002; Casas-Sainz and De Vicente, 2009; Cloetingh and Burov, 2011; Burov and Cloetingh, 2009), mantle dynamics (Roberts et al., 2019; Faccenna et al., 2014b) or a combination of both.

The residual topography map for Iberia (Fig. 8) is overall positive, with a maximum of ~ 400 m over Galicia and Iberian chain-Valencia margin and negative residual of $\sim 600\text{--}700$ m is found for the Pyrenees. Filtered free air gravity shows a positive signal over the entire peninsula with more pronounced feature of up to ~ 500 m over the Atlantic and Galicia and negative signal confined to Gibraltar. The dynamic topography map shows mainly a negative signal, with pronounced positive features over the Iberia chain – Valencia Gulf and Gibraltar and south Portugal.

Over the Iberian chain we observe positive residual and dynamic topography over the eastern side, the Iberia chain-Valencia Gulf. In this region, the Iberian chain experience recent surface uplift of ~ 500 m, forming a large dome over the last ~ 3 Ma (Scotti et al., 2014) at average rates of 0.1–0.2 mm/yr. Geodesy shows uplift over Galicia, the Central system, and the Betics (Fig. 1). Surface uplift occurred after the main shortening event and therefore cannot be linked directly to crustal thickness variation. The presence of recent intraplate volcanism (e.g., Calatrava volcanic field; Cebriá and Lopez-Ruiz, 1995) in south east Iberia provides evidence for the idea of mantle support of topography.

4. Contribution of dynamic topography in the Mediterranean regions

The spectral character and amplitudes of dynamic topography have been debated (Braun, 2010; Flament et al., 2013; Winterbourne et al., 2014; Hoggard et al., 2016), including for the case of the Mediterranean (Carminati et al., 2009; Faccenna et al., 2014a, Faccenna et al., 2014b; Boschi et al., 2010; Molnar et al., 2015; Gvirtzman et al., 2016), and this is in part due to the uncertainties on the determination of the isostatically compensated/residual topography component (e.g., Levandowski et al., 2014; Becker et al., 2014; Guerri et al., 2015).

At global scales, unambiguous evidence of dynamic topography is represented by the swells along several hotspot associated oceanic island chains, where surface uplift amplitudes range between 500 and 1200 m and widths between 1000 and 1500 km (e.g., Wilson, 1961; Morgan, 1965, 1971; Ribe and Christensen, 1994; King and Adam, 2014). The Hawaiian chain, for example, shows a topographic swell of more than ~ 1200 m (King and Adam, 2014). Global comparison between the expected (from a reference model) and observed seafloor depth also provide residual anomalies with amplitudes of $\sim \pm 1000$ m and wavelengths of 10^3 km (Hoggard et al., 2016). However, the choice of reference oceanic seafloor model and the presence of local crustal heterogeneity may be relevant (e.g. Nagihara et al., 1996; Yang et al., 2017; Yang and Gurnis, 2016).

Estimates of dynamic topography on continents is more complicated by the layered rheology and thick lithosphere (Morgan, 1965; Burov and Guillou-Frottier, 2005; Griffith et al., 1989; Sembroni et al., 2017).

However, in some cases, it is possible to document surface uplift. A nice example is represented by low amplitude (few tens of meters) - large doming in the eastern US producing uplift of the Pliocene marine deposits which is attributed to the combined effect of large-scale mantle flow and post-glacial rebound (Rowley et al., 2013a, Rowley et al., 2013b). Large-scale flooding, as during the upper Cretaceous for North America, has also been used to calibrate mantle dynamics effects related to the subduction and slab flattening in North America (Gurnis, 1990, 1993; Liu et al., 2008). The South African plateau has been interpreted as related to large scale mantle upwelling (e.g., Lithgow-Bertelloni and Silver, 1998), but the timing and amplitude is debated (Gurnis et al., 2000; Forte et al., 2010; Moucha and Forte, 2011). In Africa, localized intraplate domes have been deduced from the geological record (Burke, 1996; Zhang et al., 2012; Flament et al., 2014) and from river profile analysis (Paul et al., 2014; Rudge et al., 2015). The best documented example is the 1000 km large swell of the Blè dome of Angola showing a Quaternary uplift of marine deposit at ~500 m elevation with rates of ~2 mm yr⁻¹ (Walker et al., 2016).

4.1. Interpretation of subduction and orogeny related topography in the Mediterranean region

4.1.1. Subduction zone topography

In the Europe-Mediterranean domain clear examples of subduction-related topography are represented by the active subduction zones, as in the Calabrian-Tyrrhenian or Hellenic, but also in regions where subduction has ceased. In general, the effect of dynamic topography in subduction zones may be relevant since convection is expected to be particularly vigorous and lithospheric strength is likely reduced (e.g. Zhong and Gurnis, 1994; Hyndman and Currie, 2011; Cramer et al., 2017). However, the accuracy of determining dynamic contributions to topography is hampered by contemporaneous crustal deformation. The pull exerted by the subducting slab and the induced return flow is expected to depress the upper plate topography by some hundreds of meters outside the subduction fault region (Zhong and Gurnis, 1994). Subduction zone deformation may lead to marked topographic signals. Beneath Calabria, where subduction of Ionian lithosphere is active, the residual and the dynamic topography is negative, ~-500 m, and fast surface uplift occurs in the forearc high or in the inner portion of the wedge (e.g., Ferranti et al., 2006; Olivetti et al., 2012). The same holds for the Hellenic subduction zone (e.g., Ott et al., 2019). This pattern of negative residual/dynamic topography over subduction zone is also seen elsewhere, for example in the Cascades (Becker et al., 2014, 2015) or in Japan, and agrees well with model predictions for subduction zones in general (Zhong and Gurnis, 1994; Billen and Gurnis, 2005). The uplift rate in the forearc high may be explained by deep crustal accretion and duplexing (e.g., Minelli and Faccenna, 2010).

In the backarc region, as in the Tyrrhenian, Aegean, or Pannonian basin, residual topography is positive, ~300 m, and dynamic topography is also positive (with the exception of the Tyrrhenian Sea). However, the dynamic positive signal is usually shifted further away from the subduction zone by ~100–200 km with respect to the residual (Fig. 9). This difference, if confirmed on other convergent margin, may indicate that closer to trench the shallow upper plate may be experiencing a localized upwelling decoupled from subduction.

In the Mediterranean, we also see active continental subduction/delamination, as in the Northern Apennines and Dinarides. As for oceanic subduction, also in those regions we have a predominant negative signal for residual and dynamic topography with a positive moderate surface uplift due to crustal accretion (e.g., Piana Agostinetti and Faccenna Handy et al., 2019).

4.1.2. Slab break-off topography

Fast uplift is expected for a decrease of slab pull as in the case of slab breakoff (van Hunen and Allen, 2011; Duretz and Gerya, 2013; Bercovici et al., 2015; Garzanti et al., 2018). This is because slab sinker

removal will reduce the downward pull on the surface. During slab break off the residual should be negative but progressively reduced over time toward neutral. Surface uplift would be strongly positive and dynamic topography could be variable and change during the process. At the initial stage of slab detachment the dynamic topography is expected to be negative and then getting positive over time while the broken portion of the slab sinks into the mantle. The Central Apennines represents an excellent example of how topography adjusts to slab breakoff (Gvirtzman and Nur, 1999; Wortel and Spakman, 2000; Faccenna et al., 2014b). Here, in contrast to Calabria and the Northern Apennines, there is no evidence of deep earthquakes and compressional deformation ended in the Pleistocene. Both residual and dynamic topography are positive, ~400 m. Geodetic uplift rates are ~0.2 mm/yr (Faccenna et al., 2014b). Lower Pleistocene Marine deposits at high elevation show a surface uplift of ~1000 m or more (Pizzi, 2003).

The uplift of the Alps has been attributed to a combination of processes (e.g., Sternai et al., 2019), including slab break-off (e.g., Piromallo and Faccenna, 2004) erosion or post-glacial rebound which may be dominant (Mey et al., 2016; Sternai et al., 2019). A fraction of the fast uplift rate of the Western Alps has been attributed to deeper processes, such as slab break off (Fox et al., 2015; Sternai et al., 2019). Along the Alpine arc, the Moho and the topography show a similar trend suggesting that the Alps has the required isostatic crustal roots in correspondence of the highest peaks. The residual topography, even if small, is slightly negative and the dynamic topography is likewise negative. This would suggest that the Alps are moving upward, restoring an isostatic equilibrium after slab breakoff. In other words, the Alpine topography would have been first depressed by the load of the slab that, once released, could produce a vertical surface motion to restore isostasy. The remaining presence of a negative buoyancy sinker would still provide a negative dynamic topography signal. The Alps are an example that shows that the sign of the dynamic topography does not control the sign of surface elevation change. Uplift may well occur over a subduction zone or downwelling, with negative dynamic topography, if the downwelling pull decreases. Vice versa, we could have subsidence on site of the mantle upwelling if the rate is decreasing, although many active tectonic regions appear biased toward uplift (e.g. Becker et al., 2014, 2015).

Anatolia has also been interpreted as a case of slab break off (Keskin, 2003; Faccenna et al., 2006, Faccenna et al., 2014a, 2014b; Schildgen et al., 2014) and/or lithospheric delamination (Gogus, and Pysklywec, 2008; Komut et al., 2012; Göğüş et al., 2017). In southern Anatolia, residual topography is positive at some hundreds of meters. The presence of Upper Miocene and Early Pleistocene marine deposits in southern Taurides at elevations of ~2000 m and ~1200 m, respectively, document an elevated and variable uplift rate (Schildgen et al., 2014).

4.2. Intraplate topography and localized mantle upwelling

In the Europe-Mediterranean domain clear examples of plume-related topography are represented by the focused volcanic spots in the Eifel and Massif Central or Bohemian massif. Those regions are characterized by a positive residual (up to 1000 m) and dynamic (up to 800 m) topography over a few hundreds of kilometers extent domes, and geological surface uplift rates ranging from 0.06 to 0.25 mm/yr. Those values of surface uplift in the European-Mediterranean hot spots are at the lower end of the ones observed along oceanic hotspot oceanic island chains (King and Adam, 2014). Similar rates, wavelengths and amplitudes are found in south-eastern Iberia-Iberia chain (e.g., Scotti et al., 2014; Giachetta et al., 2015, Roberts, 2019). The average high elevation of Iberia might be related to few localized small-scale positive features, bounding internally drained basins.

The High Atlas may also fall into this category, even if crustal deformation was active there during the Neogene. Surface uplift in the High and Middle Atlas is significant as attested to by Upper Miocene

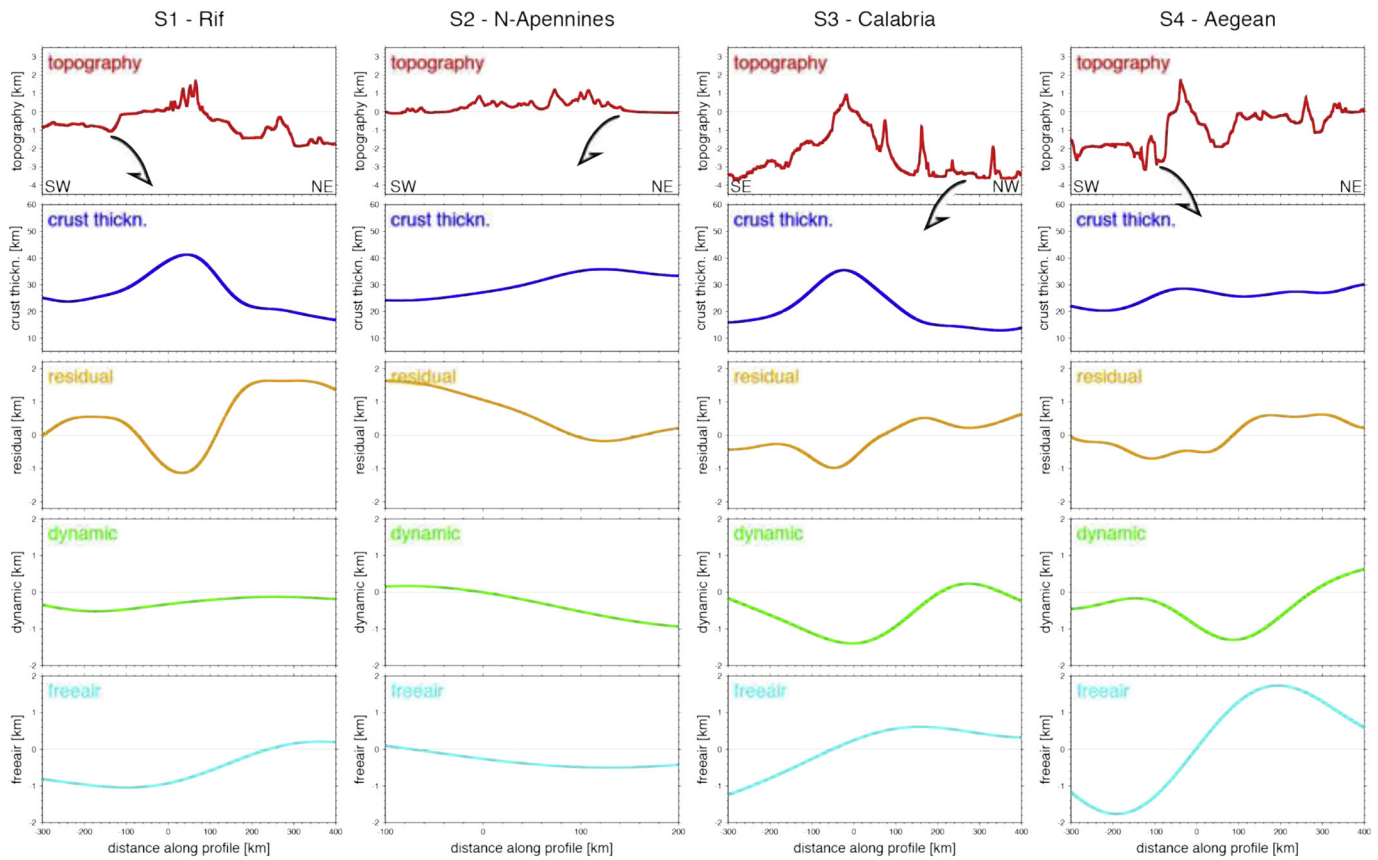


Fig. 9. Profiles of topography, smoothed crustal thickness, residual topography (Fig. 4b), flow induced dynamic (Fig. 5c), and free-air inferred (Fig. 4c) dynamic topography for four subduction related settings as indicated in profiles S1-S4 in Fig. 2a. Arrows indicates the position of the subduction zones.

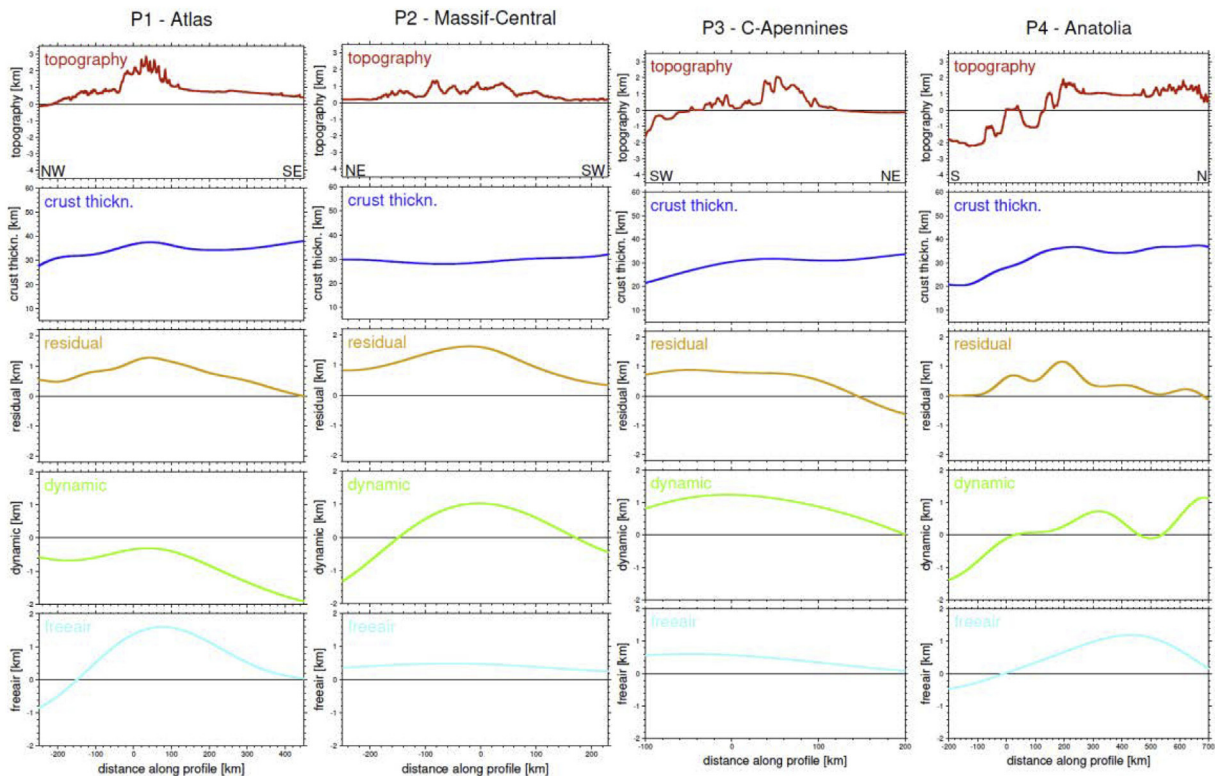


Fig. 10. Profiles of topography, smoothed crustal thickness, residual topography (Fig. 4b), flow induced dynamic (Fig. 5c), and free-air inferred (Fig. 4c) dynamic topography for four plume/slab detachment related settings as indicated in profiles P1-P4 in Fig. 2a.

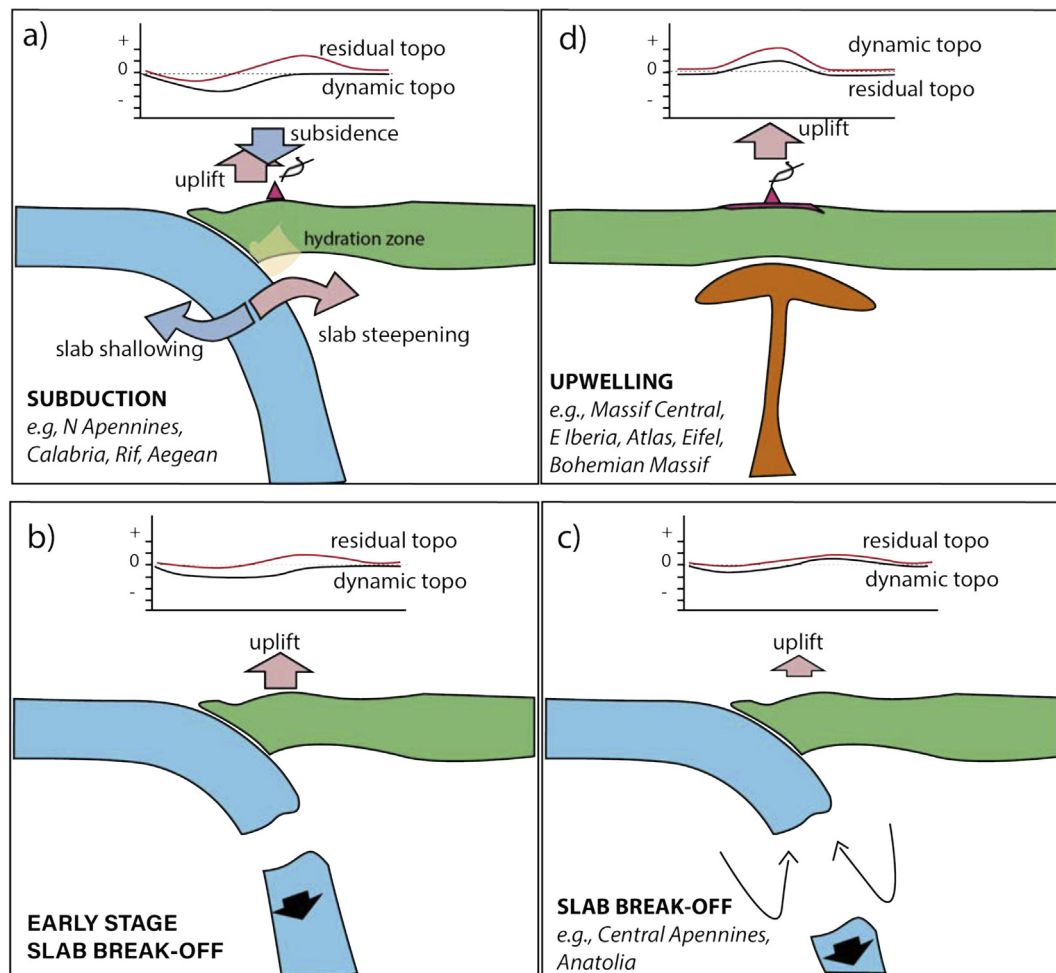


Fig. 11. Cartoon illustrating the topographic fingerprints of different dynamic setting.

marine deposits standing at high elevation (Babault et al., 2008) and by the large residual topography suggesting a mantle-supported topography swell (Duggen et al., 2009; Miller and Becker, 2014; Sun et al., 2014). A mantle origin is also implied by large volcanic fields over the Sirua and Sagro province, active in the Neogene and showing a composition similar to the Canary Islands (Duggen et al., 2009).

In summary, the Mediterranean shows well-documented examples of topography that may be due to mantle upwellings, producing small-scale domes (< 500 km) with low amplitude surface uplift (< 600 m) at rates of 0.01–0.5 mm/yr.

Based on these regional examples, we can summarize the different possible tectonic configurations that we can find in the European-Mediterranean region along with their topographic fingerprints (Fig. 11). Plume-related topography is perhaps most straightforward, with positive residual, dynamic, (slow) uplift rates and no crustal deformation. Subduction zone configurations are more complex. Actively retreating subduction typically has a negative residual and dynamic topography in the forearc region and positive residual in the backarc. In the forearc, crustal thickening and deep duplexing occurs producing positive surface uplift. If the slab is deformed, by tearing or break-off, then the pattern of topography contribution may dramatically change. At early stages of break-off, the dynamic topography is negative like the residual but the uplift rate increases, moving the forearc to an isostatic configuration. However, after a few million years, the detached slab is expected to sink deeper into the mantle while the dynamic topography signal gets progressively positive.

The amplitude of the topographic expression of mantle processes has been subject of debate. In the Mediterranean, the amplitude of the

residual topography is of the order of several hundreds of meters, ranging from 1000 m to –600 m. The amplitude of the cumulative vertical motion is also large, on average ~ 500 m, but with peaks of more than 1000 m. Therefore, areas with positive or negative residual topography show significant positive and negative recent topography variation. Regions with marked residual topography thus correspond to significant vertical motion of the surface during the last myr. Uplift rates are on average 0.2 mm/yr, and the spatial wavelengths are on average ~ 400 km for the regional tectonic processes discussed here.

5. Conclusions

A comparative analysis of residual and dynamic topography along with geodetically and geologically constrained recent uplift rates can serve to provide a more comprehensive assessment of the underlying processes that sculpt the Earth's surface. This “fingerprinting” concept can be applied to the Mediterranean. As elsewhere, active subduction is found to show an alternating negative and positive residual topography across the trench. However, the Mediterranean also provides a sampling for different stages of the transition between oceanic subduction and continental collision, including slab break-off, and forcing by positively buoyant plume anomalies leading to intraplate orogeny and swells. These cases are associated with intermediate wavelength (~200 km to 1000 km), but sometimes high amplitude (up to ~1 km) anomalous topography which is built at rates of ~0.1 to 1 mm/yr. We present a case for an important role of the mantle in driving topography across plate boundaries and within continental interiors. Further application of this fingerprint concept with more realistic lithospheric

models and additional geological and geodetic constraints provides a promising way forward to read topography for tectonic process.

Declaration of Competing Interest

We declare no Conflict of Interest.

Acknowledgement

Discussions with Sean Willett helped shaped several of the ideas on how topography is expressed as discussed here. More generally, this work summarize some of the work done over the years by our collaborators and colleagues (Morocco: Riccardo Lanari; Iberian chain: Valentina Scotti; Massif Central: Valerio Olivetti; Apennines: Malwina San Josè; Ethiopia: Andrea Sembroni and Emanuele Giachetta) and providing suggestions and comments on geomorphology (Paola Molin, Frank Pazzaglia), thermochronology (Giuditta Fellin), geodesy (Enrico Serpelloni), seismology (Claudio Chiarabba, Claudia Pìromallo, Meghan S. Miller, Lapo Boschi), geodynamics (Arthur Briaud, Nicolas Coltice, Francesca Funicello, Laurent Husson, Bernhard Steinberger), and geology (Paolo Ballato, Antonio Casas Sainz, Domenico Cosentino, Zohar Gvirtzman, Laurent Jolivet, Federico Rossetti). We wish to thank them all and many others not listed here. We would like also to acknowledge Nicolas Flament and two other, anonymous reviewers for constructive and detailed comments. CF received support from Dipartimento di Eccellenza (MIUR-Italy) grant, and TWB was partially supported by NASAOSP 201601412-001.

Appendix A. Supplementary data

Supplementary data to this article can be found online at <https://doi.org/10.1016/j.earscirev.2020.103327>.

References

- Abgarmi, B., Delph, J.R., Ozacar, A.A., Beck, S.L., Zandt, G., Sandvol, E., Biryol, C.B., 2017. Structure of the crust and African slab beneath the central Anatolian plateau from receiver functions: New insights on isostatic compensation and slab dynamics. *Geosphere* 13 (6), 1774–1787.
- Arnould, M., Coltice, N., Flament, N., Seigneur, V., Müller, R.D., 2018. On the scales of dynamic topography in whole-mantle convection models. *Geochem. Geophys. Geosyst.* 19 (9), 3140–3163.
- Auer, L., Boschi, L., Becker, T.W., Nissen-Meyer, T., Giardini, D., 2014. Savani: a variable-resolution whole-mantle model of anisotropic shear-velocity variations based on multiple datasets. *J. Geophys. Res. Solid Earth* 119. <https://doi.org/10.1002/2013JB010773>.
- Ayarza, P., Carbonell, R., Teixell, A., Palomeras, I., Martí, D., Kchikach, A., Hanafi, M., Levander, A., Gallart, J., Arboleya, M.L., Alcalde, J., Charroud, M., Amrhar, M., 2014. Crustal thickness and velocity structure across the Moroccan Atlas from long offset wide-angle reflection seismic data: the SIMA experiment. *Geochem. Geophys. Geosyst.* 15, 1698–1717. <https://doi.org/10.1002/2013GC005164.G3>.
- Babault, J., Teixell, A., Arboleya, M.L., Charroud, M., 2008. A late Cenozoic age for long wavelength surface uplift of the Atlas Mountains of Morocco. *Terra Nova* 20, 102–107. <https://doi.org/10.1111/j.1365-3121.2008.00794.x>.
- Bartol, J., Govers, R., 2014. A single cause for uplift of the Central and Eastern Anatolian plateau? *Tectonophysics* 637, 116–136.
- Beaumont, C., Kooi, H., Willett, S., 2000. Coupled tectonic-surface process models with applications to rifted margins and collisional orogens. In: *Global Tectonics*, Summerfield MA (Ed.), Geomorphology and Ed. Wiley, Chichester, pp. 29–55.
- Becker, T.W., Faccenna, C., Humphreys, E.D., Lowry, A.R., Miller, M.S., 2014. Static and dynamic support of western United States topography. *Earth Planet. Sci. Lett.* 402, 234–246.
- Becker, T.W., Lowry, A.R., Faccenna, C., Schmandt, B., Borsa, A., Yu, C., 2015. Western US intermountain seismicity caused by changes in upper mantle flow. *Nature* 524 (7566), 458–461.
- Bercovici, D., Schubert, G., Ricard, Y., 2015. Abrupt tectonics and rapid slab detachment with grain damage. *Proc. Natl. Acad. Sci.* 112 (5), 1287–1291.
- Billen, M.I., Gurnis, M., 2005. Constraints on subducting plate strength within the Kermadec trench. *J. Geophys. Res. Solid Earth* 110.
- Bird, P., 2003. An updated digital model of plate boundaries. *Geochem. Geophys. Geosyst.* 4 (3).
- Bishop, P., 2007. Long-term landscape evolution: linking tectonics and surface processes. *Earth Surface Processes and Landforms* 3 (2007), 329–365.
- Bodur, O., Rey, P., 2019. The impact of rheological uncertainty on dynamic topography predictions. *Solid Earth* 10 (6), 2167–2178.
- Bonnet, S., Crave, A., 2003. Landscape response to climate change: Insights from experimental modeling and implications for tectonics versus climatic uplift of topography. *Geology* 31, 123–126.
- Boschi, L., Faccenna, C., Becker, T.W., 2010. Mantle structure and dynamic topography in the Mediterranean Basin. *Geophys. Res. Lett.* 37, L20303. <https://doi.org/10.1029/2010GL045001>.
- Braun, J., 2010. The many surface expressions of mantle dynamics. *Nat. Geosci.* 3 (12), 825.
- Burke, K., 1996. The African plate. *J. Afr. Earth Sci.* 99, 341–409.
- Burov, E., Cloetingh, S., 2009. Controls of mantle plumes and lithospheric folding on modes of intraplate continental tectonics: differences and similarities. *Geophys. J. Int.* 178 (3), 1691–1722.
- Burov, E., Gerya, T., 2014. Asymmetric three-dimensional topography over mantle plumes. *Nature* 513, 85–89. <https://doi.org/10.1038/nature13703>.
- Burov, E., Guillou-Frotier, L., 2005. The plume-head continental lithosphere interaction using a tectonically realistic formulation for the lithosphere. *Geophys. J. Int.* 58. <https://doi.org/10.1111/j.1365-246x.2005.02588.x>.
- Carminati, E., Doglioni, C., 2012. Alps vs. Apennines: the paradigm of a tectonically asymmetric Earth. *Earth Sci. Rev.* 112, 67–96.
- Carminati, E., Martinelli, G., 2002. Subsidence rates in the Po Plain, northern Italy: the relative impact of natural and anthropogenic causation. *Eng. Geol.* 66 (3–4), 241–255.
- Carminati, E., Doglioni, C., Scrocca, D., 2003. Apennines subduction-related subsidence of Venice (Italy). *Geophys. Res. Letters* 30 (13), 1717. <https://doi.org/10.1029/2003GL017001>.
- Carminati, E., Cuffaro, M., Doglioni, C., 2009. Cenozoic uplift of Europe. *Tectonics* 28 (4).
- Carminati, E., Lustrino, M., Doglioni, C., 2012. 2012. Geodynamic evolution of the central and western Mediterranean: Tectonics vs. igneous petrology constraints. *Tectonophysics*. <https://doi.org/10.1016/j.tecto.2012.01.026>.
- Casas-Sainz, A., De Vicente, G., 2009. On the tectonic origin of Iberian topography. *Tectonophysics* 474 (1–2), 214–235.
- Casas-Sainz, A.M., Faccenna, C., 2001. Tertiary compressional deformation of the Iberian Plate. *Terra Nova* 13, 281–288.
- Cebriá, J.-M., Lopez-Ruiz, J., 1995. Alkali basalts and leucitites in an extensional intra-continental plate setting: the late Cenozoic Calatrava volcanic province (Central Spain). *Lithos* 35 (1–2), 27–46.
- Chiarabba, C., Jovane, L., Di Stefano, R., 2005. A new view of the Italian seismicity using 20 years of instrumental recordings. *Tectonophysics* 395, 251–268.
- Civiero, C., Strak, V., Custódio, S., Silveira, G., Rawlinson, N., Arroucau, P., Corela, C., 2018. A common deep source for upper-mantle upwellings below the Ibero-western Maghreb region from teleseismic P-wave travel-time tomography. *Earth Planet. Sci. Lett.* 499, 157–172. <https://doi.org/10.1016/j.epsl.2018.07.024>.
- Cloetingh, S., Burov, E., 2011. Lithospheric folding and sedimentary basin evolution: a review and analysis of formation mechanisms. *Basin Res.* 23 (3), 257–290.
- Cloetingh, S.A.P.L., Burov, E., Beekman, F., Andeweg, B., Andriessen, P.A.M., Garcia-Castellanos, D., 2002. Lithospheric folding in Iberia. *Tectonics* 21 (5) (5–1).
- Colli, L., Ghelichkhan, S., Bunge, H.P., 2016. On the ratio of dynamic topography and gravity anomalies in a dynamic Earth. *Geophys. Res. Lett.* 43. <https://doi.org/10.1002/2016GL067929>.
- Cosentino, D., Schildgen, T.F., Cipollari, P., Faranda, C., Gliozzi, E., Hudáčeková, N., Lucifora, S., Strecker, M.R., 2012. Late Miocene surface uplift of the southern margin of the Central Anatolian Plateau, Central Taurides, Turkey. *Geological Society of America Bulletin* 124 (1–2), 133–145.
- Craig, T.J., Jackson, J.A., Priestley, K., McKenzie, D., 2011. Earthquake distribution patterns in Africa: their relationship to variations in lithospheric and geological structure, and their rheological implications. *Geophys. J. Int.* 185 (1), 403–434.
- Cramer, F., Lithgow-Bertelloni, C.R., Tackley, P.J., 2017. The dynamical control of subduction parameters on surface topography. *Geochem. Geophys. Geosyst.* 18, 1661–1687.
- D'Agostino, N., Selvaggi, G., 2004. Crustal motion along the Eurasia-Nubia plate boundary in the Calabrian Arc and Sicily and active extension in the Messina Straits from GPS measurements. *Journal of Geophysical Research: Solid Earth* 109 (B11).
- D'Agostino, N., Jackson, J.A., Dramis, F., Funicello, R., 2001. Interactions between mantle upwelling, drainage evolution and active normal faulting: an ex-ample from the central Apennines (Italy). *Geophys. J. Int.* 147 (2), 475–497. <https://doi.org/10.1046/j.1365-246X.2001.00539.x>.
- Davies, D.R., Valentine, A.P., Kramer, S.C., Rawlinson, N., Hoggard, M.J., Eakin, C.M., Wilson, C.R., 2019. Earth's multi-scale topographic response to global mantle flow. *Nat. Geosci.* 12 (10), 845–850. <https://doi.org/10.1038/s41561-019-0441-4>.
- Davila, F.M., Lithgow-Bertelloni, C., Gimenez, M., 2010. Tectonic and dynamic controls on the topography and subsidence of the Argentine Pampas: the role of the flat slab. *Earth Planet. Sci. Lett.* 295 (1–2) (187–19).
- DeMets, C., Gordon, R.G., Argus, D.F., 2010. Geologically current plate motions. *Geophysical Journal International* 181 (1), 1–80.
- Di Stefano, R., et al., 2011. Three-dimensional Moho topography in Italy: New constraints from receiver functions and controlled source seismology. *Geochemistry, Geophysics, Geosystem* 12 (9), Q09006.
- Diaperia, G., Cammarano, F., Faccenna, C., 2019. Thermal structure of a vanishing subduction system: an example of seismically-derived crustal temperature along the Italian peninsula. *Geophysical Journal International* 219 (1), 239–247.
- Diaz, J., Gallart, J., Carbonell, R., 2016. Moho topography beneath the Iberian-Western Mediterranean region mapped from controlled-source and natural seismicity surveys. *Tectonophysics* 692, 74–85.
- Doglioni, C., Merlini, S., Cantarella, G., 1999. Foredeep geometries at the front of the Apennines in the Ionian Sea (central Mediterranean). *Earth and Planetary Science Letters* 168 (3–4), 243–254.

- Duggen, S., Hoernle, K.A., Hauff, F., Klügel, A., Bouabdellah, M., Thirlwall, M.F., 2009. Flow of Canary mantle plume material through a subcontinental lithospheric corridor beneath Africa to the Mediterranean. *Geology* 37, 283–286. <https://doi.org/10.1130/G25426A.1>.
- Duretz, T., Gerya, T.V., 2013. Slab detachment during continental collision: Influence of crustal rheology and interaction with lithospheric delamination. *Tectonophysics* 602, 124–140.
- Duretz, T., Gerya, T., Spakman, W., 2014. Slab detachment in laterally varying subduction zones: 3D numerical modeling. *Geophys. Res. Lett.* <https://doi.org/10.1002/2014GL059472>.
- Ebinger, C.J., Sleep, N.H., 1998. Cenozoic magmatism throughout East Africa resulting from impact of a single plume. *Nature* 395 (6704), 788–791. <https://doi.org/10.1038/27417>.
- England, P., Molnar, P., 1990. Surface uplift, uplift of rocks, and exhumation of rocks. *Geology* 18 (12), 1173–1177.
- Faccenna, C., Molin, P., Orecchio, B., Olivetti, V., Bellier, O., Funicello, F., ... Billi, A., 2011. Topography of the Calabria subduction zone (southern Italy): Clues for the origin of Mt. Etna. *Tectonics* 30 (1).
- Faccenna, C., Becker, T.W., Jolivet, L., Keskin, M., 2013. Mantle convection in the Middle East: Reconciling Afar upwelling, Arabia indentation and Aegean trench rollback. *Earth Planet. Sci. Lett.* 375, 254–269.
- Faccenna, C., Becker, T.W., Auer, L., Billi, A., Boschi, L., Brun, J.P., Capitanio, F.A., Funicello, F., Horváth, F., Jolivet, L., Piromallo, C., Royden, L., Rossetti, F., Serpelloni, E., 2014a. Mantle dynamics in the Mediterranean. *Rev. Geophys.* <https://doi.org/10.1002/2013RG000444>.
- Faccenna, C., Becker, T., Miller, M.S., Serpelloni, E., Willett, S.D., 2014b. Isostasy, dynamic topography, and the elevation of the Apennines of Italy. *Earth Planet. Sci. Lett.* 407, 163–174.
- Faccenna, C., Glišović, P., Forte, A., Becker, T.W., Garzanti, E., Sembroni, A., Gvirtzman, Z., 2019. Role of dynamic topography in sustaining the Nile River over 30 million years. *Nat. Geosci.* 12, 1012–1017.
- Ferranti, L., et al., 2006. Markers of the last interglacial sea level highstand along the coast of Italy: Tectonic implications. *Quat. Int.* 145–146, 30–54.
- Flament, N., Gurnis, M., Müller, R.D., 2013. A review of observations and models of dynamic topography. *Lithosphere* 5 (2), 189–210.
- Flament, N., Gurnis, M., Williams, S., Seton, M., Skogseid, J., Heine, C., Müller, R.D., 2014. Topographic asymmetry of the South Atlantic from global models of mantle flow and lithospheric stretching. *Earth Planet. Sci. Lett.* 387, 107–119.
- Flament, N., Gurnis, M., Müller, R.D., Bower, D.J., Husson, L., 2015. Influence of subduction history on south American topography. *Earth Planet. Sci. Lett.* 430, 9–18.
- Forte, A.M., 2000. Seismic-geodynamic constraints on mantle flow: implications for layered convection, mantle viscosity, and seismic anisotropy in the deep mantle. *Geophysical Monograph-American Geophysical Union* 117, 3–36.
- Forte, A.M., et al., 2009. Deep-mantle contributions to the surface dynamics of the north American continent. *Tectonophysics.* <https://doi.org/10.1016/j.tecto.2009.06.010>.
- Forte, A.M., Quéré, S., Moucha, R., Simmons, N.A., Grand, S.P., Mitrova, J.X., Rowley, D.B., 2010. Joint seismic-geodynamic-mineral physical modelling of African geodynamics: a reconciliation of deep-mantle convection with surface geophysical constraints. *Earth Planet. Sci. Lett.* 295 (3–4), 329–341.
- Fox, M., Herman, F., Kissling, E., Willett, S.D., 2015. Rapid exhumation in the Western Alps driven by slab detachment and glacial erosion. *Geology* 43 (5), 379–382.
- Frizon de Lamotte, D., Saint Bezar, B., Bracène, R., Mercier, E., 2000. The two main steps of the Atlas building and geodynamics of the western Mediterranean. *Tectonics* 19, 740–761.
- Frizon de Lamotte, D., Raulin, C., Mouchot, N., Wrobel-Daveau, J.-C., Blanpied, C., Ringenbach, J.-C., 2011. The southernmost margin of the Tethys realm during the Mesozoic and Cenozoic: initial geometry and timing of the inversion processes. *Tectonics* 30. <https://doi.org/10.1029/2010TC002691>.
- García-Castellanos, D., Cloetingh, S., Balen, a, Van, b, R., 2000. Modelling the Middle Pleistocene uplift in the Ardennes-Rhenish Massif: thermo-mechanical weakening under the Eifel? *Glob. Planet. Chang.* 27, 39–52.
- Garzanti, E., Radeff, G., Malusà, M., 2018. Slab breakoff: a critical appraisal of a geological theory as applied in space and time. *Earth Sci. Rev.* 177, 303–319.
- Ghosh, A., Becker, T.W., Humphreys, E.D., 2013. Dynamics of the North American continent. *Geophysical Journal International* 194 (2), 651–669.
- Giachetta, E., Molin, P., Scotti, V.N., Faccenna, C., 2015. Plio-Quaternary uplift of the Iberian Chain (Central-Eastern Spain) from landscape evolution experiments and river profile modeling. *Geomorphology* 246 (2015), 48–67.
- Giacomuzzi, G., Civalieri, M., De Gori, P., Chiarabba, C., 2012. 3D Vs model of the upper mantle beneath Italy: Insight on the geodynamics of Central Mediterranean. *Earth Planetary Science Lett.* 335–336, 105–120.
- Gil, A., Gallart, J., Díaz, J., Carbonell, R., Levander, A., Harbafi, M., 2014. Crustal structure beneath the Rif Cordillera, NorthMorocco, from the RIFSIWide-angle reflection seismic experiment. *Geochem. Geophys. Geosyst.* 15, 4712–4733. <https://doi.org/10.1002/2014GC005485>.
- Globig, J., Fernández, M., Torne, M., Vergés, J., Robert, A., Faccenna, C., 2016. New insights into the crust and lithospheric mantle structure of Africa from elevation, geoid, and thermal analysis. *Journal of Geophysical Research: Solid Earth* 121 (7), 5389–5424.
- Goes, S., Spakman, W., Bijwaard, H., 1999. A lower mantle source for central European Vocaism. *Science* 286, 191–193.
- Gogus, O.H., Pysklywec, R.N., 2008. Mantle lithosphere delamination driving plateau uplift and synconvergent extension in eastern Anatolia. *Geology* 36, 723–726.
- Göğüş, O.H., Pysklywec, R.N., Şengör, A.M.C., Gün*, E., 2017. Drip Tectonics and the enigmatic uplift of the Central Anatolian plateau. *Nat. Commun.* <https://doi.org/10.1038/s41467-017-01611-3>.
- Gomez, F., Allmendinger, R.W., Barazangi, M., Er-Raji, A., Dahmani, M., 1998. Crustal shortening and vertical strain partitioning in the Middle Atlas Mountains of Morocco. *Tectonics* 17, 520–533.
- Gomez, F., Beauchamp, W., Barazangi, M., 2000. Role of the Atlas Mountains (Northwest Africa) within the African-Eurasian plate-boundary zone. *Geology* 28, 775–778.
- Granet, M., Wilson, M., Achauer, U., 1995. Imaging mantle plumes beneath the French Massif Central. *Earth Planet. Sci. Lett.* 136, 199–203.
- Griffiths, R.W., Gurnis, M., Eitelberg, G., 1989. Holographic measurements of surface topography in laboratory models of mantle hotspots. *Geophys. J. Int.* 96 (3), 477–495. <https://doi.org/10.1111/j.1365-246X.1989.tb06009.x>.
- Guerri, M., Cammarano, F., Connolly, J.A.D., 2015. Effects of chemical composition, water and temperature on physical properties of continental crust. *Geochem. Geophys. Geosyst.* 16 (7), 2431–2449.
- Guerri, M., Cammarano, F., Tackley, P.J., 2016. Modelling Earth's surface topography: decomposition of the static and dynamic components. *Physics of the Earth and Planetary Interiors* 261, 172–186.
- Gurnis, M., 1990. Bounds on global dynamic topography from Phanerozoic flooding of continental platforms. *Nature* 344 (6268), 754–756. <https://doi.org/10.1038/344754a0>.
- Gurnis, M., 1993. Phanerozoic marine inundation of continents driven by dynamic topography above subducting slabs. *Nature* 364, 589–593. <https://doi.org/10.1038/364589a0>.
- Gurnis, M., Mitrova, J.X., Ritsema, J., van Heijst, H.-J., 2000. Constraining mantle density structure using geological evidence of surface uplift rates: the case of the African superplume. *Geochemistry Geophysics Geosystems* 1 (7), 1–31. <https://doi.org/10.1029/1999GC000035>.
- Gvirtzman, Z., Nur, A., 1999. The formation of Mount Etna as the consequence of slab rollback. *Nature* 401 (6755), 782.
- Gvirtzman, Z., Nur, A., 2001. Residual topography, lithospheric structure and sunken slabs in the Central Mediterranean. *Earth Planet. Sci. Lett.* 187 (1–2), 117–130.
- Gvirtzman, Z., Faccenna, C., Becker, T.W., 2016. Isostasy, flexure, and dynamic topography. *Tectonophysics* 683, 255–271.
- Hager, B.H., Richards, M.A., 1989. Long-wavelength variations in Earth's geoid: physical models and dynamical implications. *Philosophical Transactions of the Royal Society of London. Series A, Mathematical and Physical Sciences* 328 (1599), 309–327.
- Hager, B.H., Clayton, R.W., Richards, M.A., Comer, R.P., Dziewonski, A.M., 1985. Lower mantle heterogeneity, dynamic topography and the geoid. *Nature* 313 (6003), 541.
- Handy, M.R., Giese, J., Schmid, S.M., Pleuger, J., Spakman, W., Onuzi, K., Ustaszewski, K., 2019. Coupled Crust-Mantle Response to Slab Tearing, Bending, and Rollback along the Dinaride-Hellenide Orogen. *Tectonics* 38 (8), 2803–2828.
- Hayes, G., 2018. Slab2 - a Comprehensive Subduction Zone Geometry Model. U.S. Geological Survey data release <https://doi.org/10.5066/F7P6VJNV>.
- van Hinsbergen, D.J.J., Vissers, R.L., Spakman, W., 2014. Origin and consequences of western Mediterranean subduction, rollback, and slab segmentation. *Tectonics* 33 (4), 393–419.
- Hoernle, K., Zhang, Yu-S., Graham, D., 1995. Seismic and geochemical evidence for large-scale mantle upwelling beneath the eastern Atlantic and western and Central Europe. *Nature (London)* 374, 34–39.
- Hoggard, M.J., White, N., Al-Attar, D., 2016. Global dynamic topography observations reveal limited influence of large-scale mantle flow. *Nat. Geosci.* 9, 456–463. <https://doi.org/10.1038/ngeo2709>.
- Holmes, A., 1944. Principles of Physical Geology 189–190. Thomas Nelson and Sons.
- van Hunen, Jeroen, Allen, Mark B., 2011. Continental collision and slab break-off: a comparison of 3-D numerical models with observations. *Earth Planet. Sci. Lett.* 302 (1–2), 27–37.
- Hyndman, R.D., Currie, C.A., 2011. Why is the North America Cordillera high? Hot backarcs, thermal isostasy, and mountain belts. *Geology* 39 (8), 783–786.
- Karabulut, H., Paul, A., Deger Ozbakir, A., Ergun, T., Senturk, Selver, 2019. A new crustal model of the Anatolia-Aegean domain: evidence for the dominant role of isostasy in the support of the Anatolian plateau. *Geophys. J. Int.* 218, 57–73.
- Karner, G.D., Watts, A.B., 1983. Gravity anomalies and flexure of the lithosphere at mountain ranges. *Journal of Geophysical Research: Solid Earth* 88 (B12), 10449–10477.
- Keskin, M., 2003. Magma generation by slab steepening and break off beneath a subduction-accretion complex: an alternative model for collision related volcanism in eastern Anatolia, Turkey. *Geophys. Res. Lett.* 30, 8046.
- King, S.D., Adam, C., 2014. Hotspot swells revisited. *Phys. Earth Planet. Inter.* 235, 66–83.
- Kiraly, A., Faccenna, C., Funicello, F., Sembroni, A., 2015. Coupling surface and mantle dynamics: a novel experimental approach. *Geophys. Res. Lett.* 42, 3863–3869. <https://doi.org/10.1002/2015GL063867>.
- Komut, T., Gray, R., Pysklywec, R., Gogus, O.H., 2012. Mantle flow uplift of western Anatolia and the Aegean: Interpretations from geophysical analyses and geodynamic modelling. *J. Geophys. Res.* 117, B11412. <https://doi.org/10.1029/2012JB009306>.
- Lachenbruch, A.H., Morgan, M., 1990. Continental extension, magmatism and elevation; formal relations and rules of thumb. *Tectonophysics* 174, 39–62.
- Lanari, R., Fellin, M.V., Faccenna, C., Balestrieri, M.L., Pazzaglia, F.J., Youbi, N., Maden, C., 2020. Exhumation and Surface Evolution of the Western High Atlas and Surrounding Regions as Constrained by Low-Temperature Thermochronology. *Tectonics* 39 (3).
- Laske, G., Masters, G., Ma, Z., Pasyanos, M., 2013. Update on CRUST1.0—A 1-degree Global Model of Earth's Crust. In *Geophys. Res. Abstr.* Vol. 15. EGU General Assembly, Vienna, Austria, pp. 2658.
- Le Stunff, Y., Ricard, Y., 1995. Topography and geoid due to mass anomalies. *Geophys. J. Int.* 122, 982–990.
- Levandowski, W., Jones, C.H., Shen, W.S., Ritzwoller, M.H., Schulte-Pelkum, V., 2014.

- Origins of topography in the western U.S.: Mapping crustal and upper mantle density variations using a uniform seismic velocity model. *J. Geophys. Res.-Solid Earth* 119, 2375–2396.
- Lithgow-Bertelloni, C., Gurnis, M., 1997. Cenozoic subsidence and uplift of continents from time-varying dynamic topography. *Geology* 25 (8), 735–738. [https://doi.org/10.1130/0091-7613\(1997\)025<0735:CSAUOC>2.3.CO;2](https://doi.org/10.1130/0091-7613(1997)025<0735:CSAUOC>2.3.CO;2).
- Lithgow-Bertelloni, C., Silver, P.G., 1998. Dynamic topography, plate driving forces and the African superwell. *Nature* 395 (6699), 269.
- Liu, L., Spasojević, S., Gurnis, M., 2008. Reconstructing Farallon plate subduction beneath North America back to the late cretaceous. *Science* 322 (5903), 934–938.
- Lucazeau, F., Vasseur, G., Bayer, R., 1984. Interpretation of heat flow data in the French Massif Central. *Tectonophysics* 103 (1–4), 99–119.
- Lucente, F.P., Chiarabba, C., Cimini, G.B., Giardini, D., 1999. Tomographic constraints on the geodynamic evolution of the Italian region. *J. Geophys. Res.* 104, 20307–20327.
- Malinverno, A., Ryan, W.B.F., 1986. Extension on the Tyrrhenian Sea and shortening in the Apennines as results of arc migration driven by sinking of the lithosphere. *Tectonics* 5, 227–245. <https://doi.org/10.1029/TC005i002p00227>.
- Faccenna, C., Bellier, O., Martinod, J., Piromallo, C., Regard, V., 2006. Slab detachment beneath eastern Anatolia: a possible cause for the formation of the North Anatolian fault. *Earth Planet. Sci. Lett.* 242, 85–97.
- McKenzie, D., 1976. The East Anatolian Fault: a major structure in eastern Turkey. *Earth Planet. Sci. Lett.* 29, 189–193.
- Meijers, M.J., Brocard, G.Y., Cosca, M.A., Lüdecke, T., Teyssier, C., Whitney, D.L., Mulch, A., 2018. Rapid late Miocene surface uplift of the Central Anatolian Plateau margin. *Earth Planet. Sci. Lett.* 497, 29–41.
- Mey, J., Scherler, D., Wickert, A.D., Egholm, D.L., Tesauro, M., Schildgen, T.F., Strecker, M.R., 2016. Glacial isostatic uplift of the European Alps. *Nat. Commun.* 7 (1), 1–10.
- Meyer, W., Stets, J., 1998. Junge Tektonik im Rheinischen Schiefergebirge und ihre Quantifizierung. *Z. Dtsch. Geol. Ges.* 149, 359–379.
- Meyer, H., Hetzel, R., Fügenschuh, B., Strauss, H., 2010. Determining the growth rate of topographic relief using in situ-produced ¹⁰Be: a case study in the Black Forest, Germany. *Earth and Planetary Science Letters* 290 (3–4), 391–402.
- Miller, M.S., Becker, T.W., 2014. Reactivated lithospheric-scale discontinuities localize dynamic uplift of the Moroccan Atlas Mountains. *Geology* 42 (1), 35–38. <https://doi.org/10.1130/G34959.1>.
- Miller, M.S., Piana Agostinetti, N., 2012. Insights into evolution the lithospheric structure of Italy from S receiver functions. *Earth Planet. Sci. Lett.* 345, 49–59.
- Miller, M.S., Allam, A.A., Becker, T.W., Di Leo, J.F., Wookey, J., 2013. Constraints on the tectonic evolution of the westernmost Mediterranean and northwestern Africa from shear wave splitting analysis. *Earth Planet. Sci. Lett.* 375, 234–243. <https://doi.org/10.1016/j.epsl.2013.05.036>.
- Milner, K., Becker, T.W., Boschi, L., Sain, J., Schorlemmer, D., Waterhouse, H., 2009. The Solid Earth Research and Teaching Environment: a new software framework to share research tools in the classroom and across disciplines. *EOS Trans. AGU* 90, 12.
- Minelli, L., Faccenna, C., 2010. Evolution of the Calabrian accretionary wedge (Central Mediterranean). *Tectonics* 29, TC4004. <https://doi.org/10.1029/2009TC002562>.
- Missenard, Y., Zeyen, H., de Lamotte, D.F., Leturmy, P., Petit, C., Sébrier, M., Saddiqi, O., 2006. Crustal versus asthenospheric origin of relief of the Atlas mountains of Morocco. *J. Geophys. Res. Solid Earth* 111, 1–13. <https://doi.org/10.1029/2005JB003708>.
- Mitrovica, J.X., Jarvis, G.T., 1985. Surface deflections due to transient subduction in a convecting mantle. *Tectonophysics* 120, 211–237. [https://doi.org/10.1016/0040-1951\(85\)90052-6](https://doi.org/10.1016/0040-1951(85)90052-6).
- Mitrovica, J.X., Beaumont, C., Jarvis, G.T., 1989a. Tilting of continental interiors by the dynamical effects of subduction. *Tectonics* 8 (5), 1079–1094. <https://doi.org/10.1029/TC008i005p01079>.
- Mitrovica, J.X., Beaumont, C., Jarvis, G.T., 1989b. Tilting of continental interiors by the dynamical effects of subduction. *Tectonics* 8 (5), 1079–1094.
- Molinari, I., Morelli, A., 2011. EPcrust: a reference crustal model for the European Plate. *Geophys. J. Int.* 185, 352–364.
- Molnar, P., England, P.C., Jones, C.H., 2015. Mantle dynamics, isostasy, and the support of high terrain. *J. Geophys. Res.* 120. <https://doi.org/10.1002/2014JB011724>.
- Morgan, W.J., 1965. Gravity anomalies and convection currents: 1. A sphere and a cylinder sinking beneath the surface of a viscous fluid. *J. Geophys. Res.* 70, 6175–6187. <https://doi.org/10.1029/JZ070i024p06175>.
- Morgan, W.J., 1971. Convection plumes in the lower mantle. *Nature* 230, 42–43.
- Moucha, R., Forte, A.M., 2011. Changes in African topography driven by mantle convection. *Nat. Geosci.* 4 (10), 707–712.
- Moucha, R., Forte, A.M., Mitrovica, J.X., Rowley, D.B., Quéré, S., Simmons, N.A., Grand, S.P., 2008. Dynamic topography and long-term sea-level variations: there is no such thing as a stable continental platform. *Earth Planet. Sci. Lett.* 271 (1–4), 101–108. <https://doi.org/10.1016/j.epsl.2008.03.056>.
- Müller, R.D., Hassan, R., Gurnis, M., Flament, N., Williams, S.E., 2018. Dynamic topography of passive continental margins and their hinterlands since the cretaceous. *Gondwana Res.* 53, 225–251.
- Nagihara, S., Lister, C.R., Sclater, J.G., 1996. Reheating of old oceanic lithosphere: deductions from observations. *Earth Planet. Sci. Lett.* 139 (1–2), 91–104.
- Olivetti, V., Cyr, A.J., Molin, P., Faccenna, C., Granger, D.E., 2012. Uplift history of the Vela Massif, southern Italy, deciphered from cosmogenic ¹⁰Be erosion rates and river longitudinal profile analysis. *Tectonics* 31, 26. <https://doi.org/10.1029/2011TC003037>. TCXXXX.
- Olivetti, V., Godard, G., Bellier, G., team, A.S.T.E.R., 2016. Cenozoic rejuvenation events of Massif Central topography (France): Insights from cosmogenic denudation rates and river profiles. *Earth Planet. Sci. Lett.* 444, 179–191. <https://doi.org/10.1016/j.epsl.2016.03.049>.
- Ott, R.F., Gallen, S.F., Wegmann, K.W., Biswas, R.H., Herman, F., Willett, S.D., 2019. Pleistocene terrace formation, Quaternary rock uplift rates and geodynamics of the Hellenic Subduction Zone revealed from dating of paleoshorelines on Crete, Greece. *Earth and Planetary Science Letters* 525.
- Panasnyuk, S.V., Hager, B.H., 2000. Models of isostatic and dynamic topography, geoid anomalies, and their uncertainties. *J. Geophys. Res.* 105 (B12), 28,199–28,209. <https://doi.org/10.1029/2000JB900249>.
- Panza, G., Raykova, R.B., Carminati, E., Doglioni, C., 2007. Upper mantle flow in the western Mediterranean. *Earth Planet. Sci. Lett.* 257, 200–214.
- Patacca, E., Sartori, R., Scandone, P., 1990. Tyrrhenian basin and Apenninic arcs: Kinematic relations since late tortonian times. *Mem. Geol. Soc. Ital.* 45, 425–451.
- Paul, J.D., Roberts, G.G., White, N., 2014. The African landscape through space and time. *Tectonics* 33, 898–935. <https://doi.org/10.1002/2013TC003479>.
- Peltier, W.R., 2004. Global Glacial Isostasy and the surface of the Ice-Age Earth: the Ice-5g (Vm2) Model and Grace. *Annu. Rev. Earth Planet. Sci.* 32 (1), 111–149.
- Piana Agostinetti, N., Amato, A., 2009. Moho depth and VP, /VS ratio in peninsular Italy from teleseismic receiver functions. 114, B06303. <https://doi.org/10.1029/2008JB005899>.
- Piana Agostinetti, N., Faccenna, C., 2018. Deep structure of Northern Apennines subduction orogen (Italy) as revealed by a joint interpretation of passive and active seismic data. *Geophys. Res. Lett.* 45 (9), 4017–4024.
- Piana Agostinetti, N., Steckler, M.S., Lucente, F.P., 2009. Imaging the subducted slab under the Calabrian Arc, Italy, from receiver function analysis. *Lithosphere* 1, 131–138. <https://doi.org/10.1130/L49.1>.
- Piromallo, C., Faccenna, C., 2004. How deep can we find the traces of Alpine subduction? *Geophys. Res. Lett.* 31 (6).
- Piromallo, C., Morelli, A., 2003. P wave tomography of the mantle under the Alpine-Mediterranean area. *J. Geophys. Res.* 108, 2065. <https://doi.org/10.1029/2002JB001757>. (B2).
- Pizzi, A., 2003. Plio-Quaternary uplift rates in the outer zone of the central Apennines fold-and-thrust belt, Italy. *Quat. Int.* 101–102, 229–237.
- Pysklywec, R.N., Mitrovica, J.X., 1997. Mantle avalanches and the dynamic topography of continents. *Earth Planet. Sci. Lett.* 148 (3–4), 447–455.
- Pysklywec, R.N., Mitrovica, J.X., 1998. Mantle flow mechanisms for the large-scale subsidence of continental interiors. *Geology* 26 (8), 687–690.
- Regard, V., Faccenna, C., Bellier, O., Martinod, J., 2008. Laboratory experiments of slab break-off and slab dip reversal: insight into the Alpine Oligocene reorganization. *Terra Nova* 20 (4), 267–273.
- Ribe, N.M., Christensen, U.R., 1994. The dynamical origin of Hawaiian volcanism. *Earth Planet. Sci. Lett.* 171, 517–531.
- Richards, M.A., Hager, B.H., 1989. Effects of lateral viscosity variations on long-wavelength geoid anomalies and topography. *J. Geophys. Res.* 94 (10), 299–313.
- Ritter, J.R.R., Jordan, M., Christensen, U.R., Achauer, U., 2001. A mantle plume below the Eifel volcanic fields, Germany. *Earth Planet. Sci. Lett.* 186, 7–14.
- Conway-Jones, B.W., Roberts, G.G., Fichtner, A., Hoggard, M., 2019. Neogene epeirogeny of Iberia. *Geochemistry, Geophysics, Geosystems* 20 (2), 1138–1163.
- Rowley, D.B., Forte, A.M., Moucha, R., Mitrovica, J.X., Simmons, N.A., Grand, S.P., 2013a. Dynamic topography change of the eastern United States since 3 million years ago. *Science* 340 (6140), 1560–1563.
- Rowley, D.B., Forte, A.M., Moucha, R., Mitrovica, J.X., Simmons, N.A., Grand, S.P., 2013b. Dynamic topography change of the eastern United States since 3 million years ago. *Science* 340 (6140), 1560–1563.
- Royden, L., 1993. The tectonic expression of slab pull at continental convergent boundaries. *Tectonics* 12, 303–325. <https://doi.org/10.1029/92TC02248>.
- Royden, L., Faccenna, C., 2018. Subduction Orogeny and the late Cenozoic Evolution of the Mediterranean Arcs. *Annu. Rev. Earth Planet. Sci.* 46 (1), 261–289 2018.
- Royden, L., Husson, L., 2006. Trench motion, slab geometry and viscous stresses in subduction systems. *Geophys. J. Int.* 167, 881–905. <https://doi.org/10.1111/j.1365-246X.2006.03079.x>.
- Rudge, J.F., Roberts, G.G., White, N.J., Richardson, C.N., 2015. Uplift histories of Africa and Australia from linear inverse modeling of drainage inventories. *J. Geophys. Res. - Earth* 120 (5), 894–914.
- Sartori, R., 1990. The main results of ODP Leg 107 in the frame of Neogene to recent geology of peritryrhenian areas. In: Kastens, K.A. (Ed.), *Proc. ODP Sci. Res.*, vol. 107. Ocean Drilling Program, College Station, Tex, pp. 715–730.
- Schildgen, T.F., Yildirim, C., Cosentino, D., Strecker, M.R., 2014. Linking slab break-off, Hellenic trench retreat, and uplift of the Central and Eastern Anatolian plateaus. *Earth Sci. Rev.* 128, 147–168.
- Scotti, V.N., Molin, P., Faccenna, C., Soligo, M., Casas-Sainz, A., 2014. The influence of surface and tectonic processes on landscape evolution of the Iberian Chain (Spain): Quantitative geomorphological analysis and geochronology. *Geomorphology* 206, 37–57. <https://doi.org/10.1016/j.geomorph.2013.09.017>.
- Sembroni, A., Faccenna, C., Becker, T.W., Molin, P., Abebe, B., 2016. Long-term, deep-mantle support of the Ethiopia-Yemen Plateau. *Tectonics* 35, 469–488. <https://doi.org/10.1002/2015TC004000>.
- Sembroni, A., Kiraly, A., Faccenna, C., Funicello, F., Becker, T.W., Globig, J., Fernandez, M., 2017. Impact of the lithosphere on dynamic topography: Insights from analogue modeling. *Geophys. Res. Lett.* 44. <https://doi.org/10.1002/2017GL072668>.
- Sengor, A.M.C., Ozeren, S., Genc, T., Zor, E., 2003. East Anatolian high plateau as a mantle-supported, north-south shortened domal structure. *Geophys. Res. Lett.* 30, 8045.
- Serpelloni, E., Faccenna, C., Spada, G., Dong, D., Williams, S.D., 2013. Vertical GPS ground motion rates in the Euro-Mediterranean region: New evidence of velocity gradients at different spatial scales along the Nubia-Eurasia plate boundary. *J. Geophys. Res.* 118, 6003–6024.
- Shephard, G.E., Müller, R.D., Liu, L., Gurnis, M., 2010. Miocene drainage reversal of the Amazon River driven by plate-mantle interaction. *Nat. Geosci.* 3 (12), 870–875.

- <https://doi.org/10.1038/ngeo1017>.
- Sobolev, S.V., Zeyen, H., Granet, M., Achauer, U., Bauer, C., Werling, F., Altherr, R., Fuchs, K., 1997. Upper mantle temperatures and lithosphere-asthenosphere system beneath the French Massif Central constrained by seismic, gravity, petrologic and thermal observations. *Tectonophysics* 275, 143–164.
- Spada, M., Bianchi, I., Kissling, E., Agostinetti, N.P., Wiemer, S., 2013. Combining controlled-source seismology and receiver function information to derive 3-D Moho topography for Italy. *Geophys. J. Int.* 194 (2), 1050–1068.
- Steinberger, B., 2007. Effects of latent heat release at phase boundaries on flow in the Earth's mantle, phase boundary topography and dynamic topography at the Earth's surface. *Physics of the Earth and Planetary Interiors* 164 (1–2), 2–20. <https://doi.org/10.1016/j.pepi.2007.04.021>.
- Steinberger, B., 2016. Topography caused by mantle density variations: observation-based estimates and models derived from tomography and lithosphere thickness. *Geophys. J. Int.* 205, 604–621. <https://doi.org/10.1093/gji/ggw040>.
- Steinberger, B., Schmeling, H., Marquart, G., 2001. Large-scale lithospheric stress field and topography induced by global mantle circulation. *Earth Planet. Sci. Lett.* 186 (1), 75–91.
- Steinberger, B., Conrad, C., Osei, Tutu Anthony, Hoggard Mark, J., 2019. On the amplitude of dynamic topography at spherical harmonic degree two. *Tectonophysics* 760 (2019), 221–228.
- Sternai, P., Sue, C., Husson, L., Serpelloni, E., Becker, T.W., Willett, S., Faccenna, C., Di Giulio, A., Spada, G., Jolivet, L., Valla, P., Petit, C., Nocquet, J.-M., Walpersdorf, A., Castellort, S., 2019. Present-day uplift of the European Alps: evaluating mechanisms and models of their relative contributions. *Earth-Sci. Rev.* 190, 589–604, 2019.
- Sun, D., Miller, M.S., Holt, A.F., Becker, T.W., 2014. Hot upwelling conduit beneath the Atlas Mountains, Morocco. *Geophys. Res. Lett.* 41, 8037–8044. <https://doi.org/10.1002/2014GL061884>.
- Teixell, A., Arbolea, M.L., Julivert, M., Charroud, M., 2003. Tectonic shortening and topography in the central High Atlas (Morocco). *Tectonics* 22, 1051. <https://doi.org/10.1029/2002TC001460>.
- Teixell, A., Ayarza, P., Zeyen, H., Fernández, M., Arbolea, M.L., 2005. Effects of mantle upwelling in a compressional setting: the Atlas Mountains of Morocco. *Terra Nova* 17, 456–461. <https://doi.org/10.1111/j.1365-3121.2005.00633.x>.
- Tesauro, M., Hollenstein, C., Egli, R., Geiger, A., Kahle, H.G., 2005. Continuous GPS and broad-scale deformation across the Rhine Graben and the Alps. *International Journal of Earth Sciences* 94 (4), 525–537.
- Tezel, T., Shibusani, T., Kaypak, B., 2013. Crustal thickness of Turkey determined by receiver function. *J. Asian Earth Sci.* 75, 36–45.
- Thurner, S., Palomeras, I., Levander, A., Carbonell, R., Cin-ty, L., 2014. Evidence for Ongoing Lithospheric Removal in the Western Mediterranean: Ps Receiver Function results from the PICASSO Project, G3. (10.002/201GC005124).
- Torne, M., Fernández, M., Vergés, J., Ayala, C., Salas, M.C., Jimenez-Munt, I., ... Díaz, J., 2015. Crust and mantle lithospheric structure of the Iberian Peninsula deduced from potential field modeling and thermal analysis. *Tectonophysics* 663, 419–433.
- Vanacore, E.A., Taymaz, T., Saygin, E., 2013. Moho structure of the Anatolian Plate from receiver function analysis. *Geophys. J. Int.* 193 (1), 329–337.
- Wager, L.R., 1933. The rise of the Himalaya. *Nature* 132 (3322), 28.
- Waldhauser, F., Kissling, E., Ansgore, J., Mueller, S., 1998. Three dimensional interface modelling with two-dimensional seismic data: the Alpine crust-mantle boundary. *Geophys. J. Int.* 135 (1), 264–278.
- Walker, R.T., Telfer, M., Kahle, R.L., Dee, M.W., Kahle, B., Schwenninger, J.L., Watts, A.B., 2016. Rapid mantle-driven uplift along the Angolan margin in the late Quaternary. *Nature Geoscience* 9 (12), 909–914.
- Whipple, K.X., 2009. The influence of climate on the tectonic evolution of mountain belts. *Nat. Geosci.* 2 (2), 97–104.
- Whipple, K.X., Meade, B.J., 2006. Orogen response to changes in climatic and tectonic forcing. *Earth Planet. Sci. Lett.* 243, 218–228.
- Willett, S.D., 1999. Orogeny and orography: the effects of erosion on the structure of mountain belts. *J. Geophys. Res.* 104, 28957–28981.
- Willett, S.D., Slingerland, R., Hovius, N., 2001. Uplift, shortening, and steady state topography in active mountain belts. *Am. J. Sci.* 301, 455–485.
- Wilson, J.T., 1966. Did the Atlantic close and then re-open? *Nature* 211 (5050), 676–681.
- Winterbourne, J., White, N., Crosby, A., 2014. Accurate measurements of residual topography from the oceanic realm. *Tectonics* 33 (6), 982–1015.
- Wortel, M.J.R., Spakman, W., 2000. Subduction and slab detachment in the Mediterranean-Carpathian region. *Science* 290, 1910–1917.
- Wüllner, U., Christensen, U.R., Jordan, M., 2006. Joint geodynamical and seismic modelling of the Eifel plume. *Geophys. J. Int.* 165, 357–372.
- Yang, T., Gurnis, M., 2016. Dynamic topography, gravity and the role of lateral viscosity variations from inversion of global mantle flow. *Geophysical Supplements to the Monthly Notices of the Royal Astronomical Society* 207 (2), 1186–1202.
- Yang, T., Moresi, L., Müller, R.D., Gurnis, M., 2017. Oceanic residual topography agrees with mantle flow predictions at long wavelengths. *Geophys. Res. Lett.* 44 (21), 10–896.
- Zhang, N., Zhong, S., Flowers, R.M., 2012. Predicting and testing continental vertical motion histories since the Paleozoic. *Earth Planet. Sci. Lett.* 317–318, 426–435. <https://doi.org/10.1016/j.epsl.2011.10.041>.
- Zhong, S., Gurnis, M., 1994. Controls on trench topography from dynamic models of subducted slabs. *J. Geophys. Res.* 99 (B8), 15,683–15,695.
- Zor, E., Sandvol, E., Gurbuz, C., Turkelli, N., Seber, D., Barazangi, M., 2003. The crustal structure of the East Anatolian plateau (Turkey) from receiver functions. *Geophys. Res. Lett.* 30, 8044.
- Öğretmen, Nazik, et al., 2018. Evidence for 1.5 km of uplift of the Central Anatolian Plateau's southern margin in the last 450 kyr and implications for its multiphased uplift history. *Tectonics* 37 (1), 359–390.